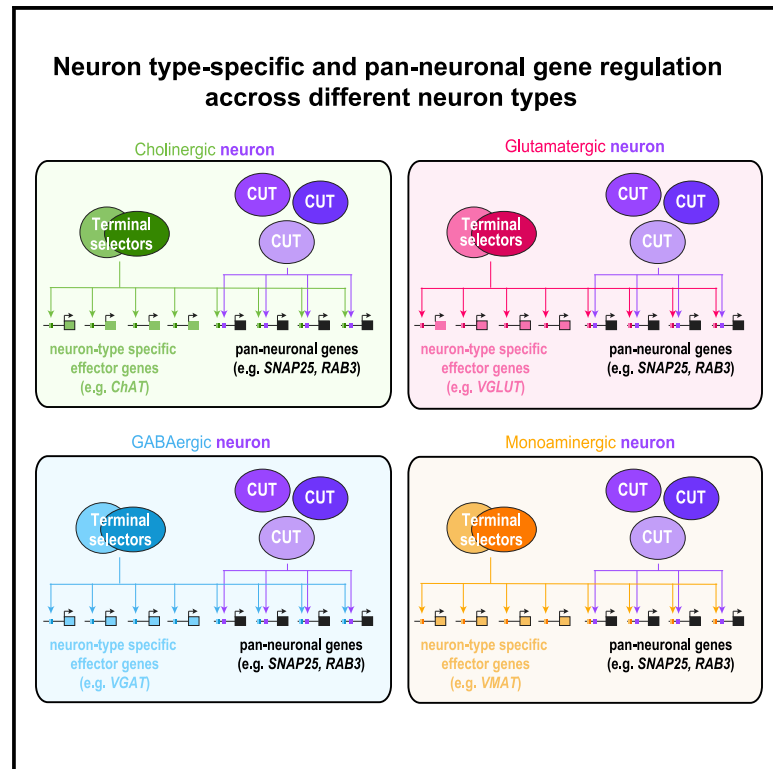


Robust regulatory architecture of pan-neuronal gene expression

Graphical abstract



Authors

Eduardo Leyva-Díaz, Oliver Hobert

Correspondence

eld2154@columbia.edu (E.L.-D.),
or38@columbia.edu (O.H.)

In brief

How do genes expressed by all neurons in a nervous system acquire their pan-neuronal specificity? Leyva-Díaz and Hobert address this long-standing question, demonstrating that pan-neuronal genes that encode, for example, synaptic vesicle proteins are controlled via a robust regulatory mechanism that deploys six members of the CUT homeobox gene family.

Highlights

- *C. elegans* CUT family homeobox genes directly control pan-neuronal gene expression
- Proper CUT gene dosage ensures robust pan-neuronal gene expression
- CUT genes are required for proper neuronal function and synapse density
- CUT genes collaborate with terminal selectors of neuron-type-specific identities



Article

Robust regulatory architecture of pan-neuronal gene expression

Eduardo Leyva-Díaz^{1,*} and Oliver Hobert^{1,2,*}¹Department of Biological Sciences, Columbia University, Howard Hughes Medical Institute, New York, NY, USA²Lead contact*Correspondence: eld2154@columbia.edu (E.L.-D.), or38@columbia.edu (O.H.)<https://doi.org/10.1016/j.cub.2022.02.040>**SUMMARY**

Pan-neuronally expressed genes, such as genes involved in the synaptic vesicle cycle or in neuropeptide maturation, are critical for proper function of all neurons, but the transcriptional control mechanisms that direct such genes to all neurons of a nervous system remain poorly understood. We show here that six members of the CUT family of homeobox genes control pan-neuronal identity specification in *Caenorhabditis elegans*. Single CUT mutants show barely any effects on pan-neuronal gene expression or global nervous system function, but such effects become apparent and progressively worsen upon removal of additional CUT family members, indicating a critical role of gene dosage. Overexpression of each individual CUT gene rescued the phenotype of compound mutants, corroborating that gene dosage, rather than the activity of specific members of the gene family, is critical for CUT gene family function. Genome-wide binding profiles, as well as mutation of CUT homeodomain binding sites by CRISPR/Cas9 genome engineering show that CUT genes directly control the expression of pan-neuronal features. Moreover, CUT genes act in conjunction with neuron-type-specific transcription factors to control pan-neuronal gene expression. Our study, therefore, provides a previously missing key insight into how neuronal gene expression programs are specified and reveals a highly buffered and robust mechanism that controls the most critical functional features of all neuronal cell types.

INTRODUCTION

To understand nervous system development, it is of critical importance to decipher the mechanisms that control the expression of neuronal gene batteries. Apart from ubiquitous housekeeping genes expressed in all tissue types, neuronal gene batteries fall into two categories: (1) genes selectively expressed in specific neuron classes; these include neurotransmitter synthesis pathway genes, individual neuropeptides genes, ion channels, signaling receptors, and many others (Figure 1A).^{1,3} (2) Pan-neuronally expressed genes that execute functions shared by all neurons but not necessarily other cell types; these genes encode proteins involved in a number of generic neuronal processes, including synaptic vesicle release (e.g., *RAB3*, *SNAP25*, and *RIM*), dense core biogenesis and release (e.g., *CAPS*), molecular motors (e.g., kinesins), or neuropeptide processing enzymes (e.g., specific endopeptidases, carboxypeptidases, and monooxygenases).^{3,4} Great strides have been made in understanding the regulation of the first category of genes, neuron-type-specific gene batteries, in the nervous system of many species.^{5–7} However, the regulatory programs that orchestrate pan-neuronal gene expression have remained elusive in any species to date.⁴ Basic helix-loop-helix transcription factors that act as proneural factors to establish neuronal identity during development are usually only transiently expressed and are therefore not good candidates to initiate and maintain pan-neuronal gene expression throughout the life of a neuron.⁸

In the nematode *Caenorhabditis elegans*, and other organisms as well, the expression of neuron-type-specific genes during terminal differentiation is controlled by neuron-type-specific combinations of terminal selector transcription factors.^{1,5,7} However, genetic removal of a terminal selector does not generally affect the expression of pan-neuronal identity features.^{1,5} For example, loss of the LIM homeobox gene *txx-3* or the EBF-type *unc-3* zinc knuckle transcription factor results in the loss of all known neuron-type-specific identity features of the cholinergic A1Y interneuron or the cholinergic ventral nerve cord motoneurons, respectively, while the expression of pan-neuronal genes remains unaffected.^{9,10} Similarly, in mice, BRNA3 and ISL1 control neuron-type-specific but not pan-neuronal features of sensory neurons of the trigeminal ganglion and dorsal root ganglia.¹¹ In an attempt to decipher the apparent parallel-acting gene regulatory programs of pan-neuronal gene expression, we have previously isolated *cis*-regulatory enhancer elements from pan-neuronally expressed genes.⁴ However, genetic screens for mutants that affect the expression of these *cis*-regulatory elements have remained unsuccessful.¹²

In this paper, we describe the discovery that six members of a specific family of homeobox genes, the CUT homeobox genes, jointly control pan-neuronal gene expression. CUT genes are expressed in all neurons and bind to the regulatory control regions of pan-neuronal genes. Deletion of the CUT homeodomain binding motif from pan-neuronal genes, using CRISPR/Cas9 genome engineering, disrupts the expression and function of



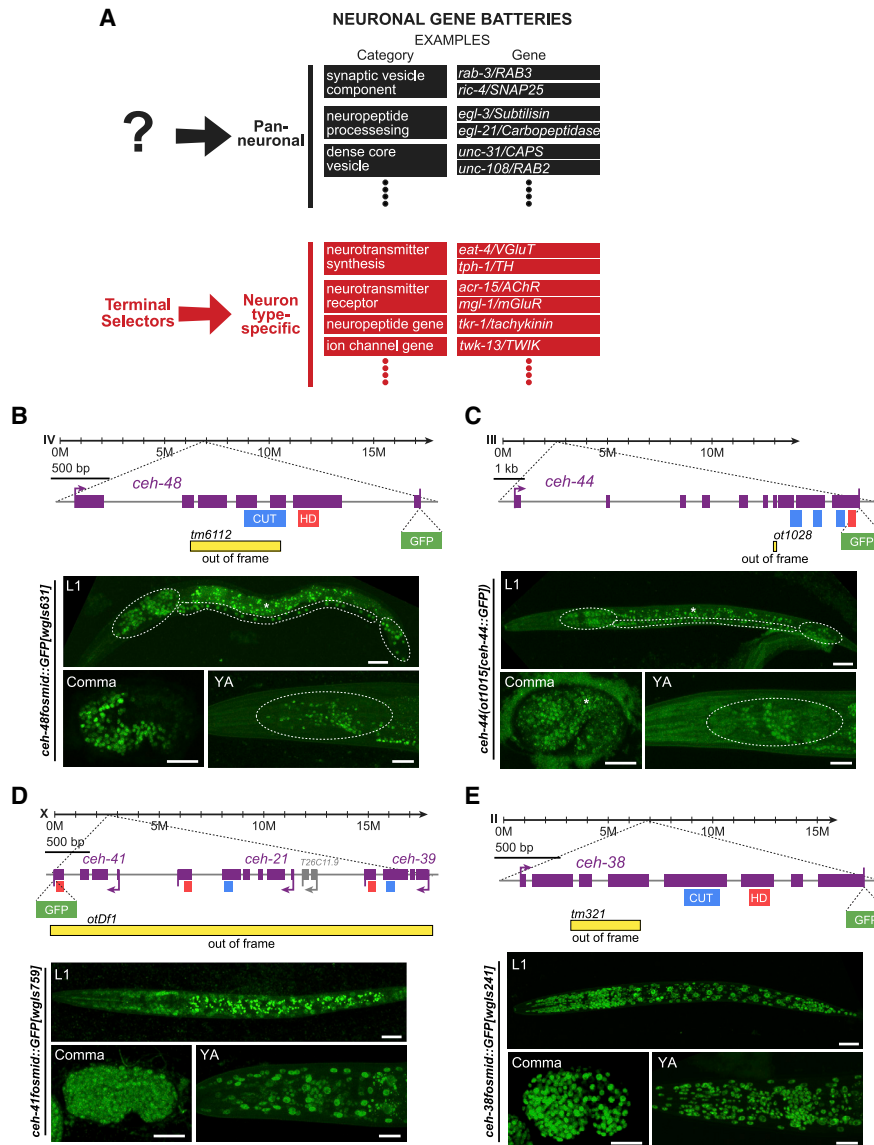


Figure 1. CUT genes are expressed pan-neuronally

(A) Schematic illustration of two main components of neuronal gene batteries, pan-neuronally expressed genes, for which no current regulator is known, and neuron-type-specific gene batteries that are controlled by terminal selector-type transcription factors.¹ Examples for genes in each category are provided. (B–E) Schematic representation of *ceh-48* (B); *ceh-44* (C); *ceh-41*, *ceh-21*, and *ceh-39* (D); and *ceh-38* (E) gene loci showing mutant alleles, GFP tags, and CUT and homeodomain motif location. Note that the *ceh-44(ot1028)* allele is designed to introduce a frameshift in the CUT homeobox isoform of the Y54F10AM.4 locus (isoform a) and does not affect the b isoform of this locus, which generates a different, non-homeodomain-containing isoform, homologous to CASP protein.² Reporter expression at the comma embryonic stage (bottom left, lateral view), L1 larval stage (top, full worm lateral views), and young adult stage (bottom right, lateral view) showing *ceh-48* (*ceh-48fosmid::GFP[wgls631]*) (B) and *ceh-44* (*ceh-44(ot1015[ceh-44::GFP]*) (C) pan-neuronal expression and *ceh-41*, *ceh-21*, and *ceh-39* (D), *ceh-38* (*ceh-38fosmid::GFP[wgls241]*) (E) ubiquitous expression. We use a fosmid reporter for *ceh-41* (*ceh-41fosmid::GFP[wgls759]*), the last gene in the operon of three ONECUT genes, which provides a readout for expression of all genes in the operon. The embryonic comma stage is the stage when neurons are born. Head ganglia, ventral nerve cord, and tail ganglia outlined in L1 images and head ganglia outlined in young adult images for *ceh-48* and *ceh-44* reporters. Asterisks (*) indicate autofluorescence in L1 (*ceh-48* and *ceh-44*) and comma (*ceh-44*) images. See Figure S1 for a comparison between CRISPR reporter expression for the different CUT genes. YA, young adult; scale bars, 15 μ m.

pan-neuronal genes. Removal of individual CUT genes reveals a dosage-sensitive function of these genes in controlling pan-neuronal gene expression and neuronal function. These phenotypes can be rescued by the expression of individual CUT factors, indicating that these factors act redundantly. A more extensive neuronal transcriptional profiling in neurons lacking

all neuronal CUT genes reveals that these factors are required for the expression of large cohorts of neuronal genes. Further genetic loss-of-function analysis reveals that pan-neuronally expressed CUT genes cooperate with neuron-type-specific terminal selectors to control pan-neuronal gene expression. Our studies reveal an exceptionally robust regulatory architecture

of pan-neuronal gene expression, which contrasts the regulation of neuron-type-specific genes, which depend on fewer regulatory inputs. Our findings may have implications for the evolution of neuronal cell-type diversity.

RESULTS

CUT homeobox genes are expressed in all neurons

Our recently reported genome-wide analysis of the expression of all homeobox genes, which are critical regulators of neuron-type-specific identity programs, uncovered a clue for potentially solving the riddle of pan-neuronal gene expression. Using both fosmid-based reporters, as well as CRISPR/Cas9-engineered reporter alleles, in which we inserted *gfp* reporter transgenes in endogenous gene loci, we found that two homeobox genes, *ceh-44* and *ceh-48*, are restricted to all neurons of the adult nervous system (Figures 1B and 1C).¹³ The only non-neuronal cells that express one of these two genes (*ceh-48*) are the secretory uv1 uterine cells, whose neuronal characters, including expression of synaptic vesicular machinery and the neurotransmitter tyramine, have been noted before.^{4,14} Expression of *ceh-44* and *ceh-48* commences right after the birth of neurons in an embryo, slightly preceding the onset of various other markers of pan-neuronal identity,⁴ and they are continuously expressed throughout the life of the organism (Figures 1B and 1C).

ceh-44 and *ceh-48* are members of the CUT family of homeobox genes, defined by the presence of a homeodomain and one or more CUT domains.¹⁵ Based on the presence of multiple CUT domains, *ceh-44* is the sole representative of the CUX subclass of the CUT family in *C. elegans*, while *ceh-48* is a member of the ONECUT subclass, characterized by the presence of a single CUT domain.² The DNA-binding sites of CUX and ONECUT homeodomain proteins are very similar.¹⁶ In addition to *ceh-48*, the *C. elegans* genome encodes five additional ONECUT genes, three of which are located in a single operon (Figure 1D). Four of these additional ONECUT genes are ubiquitously expressed in all tissues at all stages (Figures 1D and 1E), while one ONECUT gene (*ceh-49*) is only expressed in the early embryo before neurogenesis. *ceh-49* was not considered further here. Comparison of the expression level of all CUT gene loci, assessed with CRISPR/Cas9-engineered reporter alleles, shows that *ceh-38* is the most highly expressed CUT family member (Figure S1).

Binding sites for CUT homeodomain proteins are required for pan-neuronal gene expression

The pan-neuronal expression of *ceh-44* and *ceh-48* made us consider these CUT family genes as potential regulators of pan-neuronal identity. Supporting this notion, we find that many pan-neuronal genes whose *cis*-regulatory control regions we had previously defined as contributing to pan-neuronal gene expression⁴ contain predicted CUT homeodomain binding sites (as mentioned above, the DNA-binding sites of CUX and ONECUT proteins appear to be very similar,¹⁶ and from hereon, we refer to these sites as “CUT homeodomain binding sites”) (Figures 2A and S2). Moreover, animal-wide chromatin immunoprecipitation (ChIP) of CEH-48 conducted by the modENCODE consortium revealed binding of CEH-48 to these *cis*-regulatory elements (Data S1A).²¹

We assessed the functional relevance of these CUT homeodomain binding sites in two different ways: first, we deleted these sites in the context of enhancer fragments, isolated from pan-neuronal gene loci, that drive broad neuronal if not pan-neuronal expression in transgenic, multicopy reporter arrays. We observed a loss of expression upon deletion of CUT homeodomain binding sites from isolated *cis*-regulatory enhancer elements derived from the *rab-3/RAB3*, *ric-4/SNAP25*, and *unc-10/RIM* genes (Figures 2B–2E). Second, we used CRISPR/Cas9 genome engineering to first tag several pan-neuronal genes (*rab-3/RAB3*, *ric-4/SNAP25*, *unc-10/RIM*, and *ehs-1/EPS15*) with a *gfp* reporter tag and to subsequently delete their respective CUT homeodomain binding site from the respective endogenous locus. Deletion of CUT homeodomain binding sites affected the expression of all four pan-neuronal genes that we tested (Figures 2B–2E and S5D).

We tested the functional significance of the CUT homeodomain binding site mutations by asking whether these potential *cis*-regulatory alleles displayed behavioral defects that are expected from the loss of function of these pan-neuronal genes. *rab-3/RAB3* and *ric-4/SNAP25* null alleles show defects in synaptic transmission that can be measured via the sensitivity of animals to a drug that affects synaptic transmission at the neuromuscular junction, namely, aldicarb.^{22,23} We found that *rab-3/RAB3* and *ric-4/SNAP25* alleles carrying CUT homeodomain binding site mutations show resistance to aldicarb (Figure 2F), which correlates with the reduction in *ric-4/SNAP25* and *rab-3/RAB3* expression observed in these alleles and indicate impairment of synaptic transmission. Taken together, the functional relevance of presumptive CUT homeodomain binding sites hints toward a function of the CUT family of transcription factors as potential regulators of pan-neuronal gene expression.

Dosage-dependent requirement of CUT homeobox genes for pan-neuronal gene expression and neuronal behavior

We next analyzed the consequences of genetic removal of the two pan-neuronally expressed *ceh-44* and *ceh-48* genes. We used a *ceh-48* null allele from a *C. elegans* knockout consortium²⁴ and engineered a *ceh-44* null allele using the CRISPR/Cas9 system (Figures 1B and 1C). As the first step to assess gene function, we analyzed the expression of a *rab-3* reporter construct in single and double *ceh-44* and *ceh-48* null mutant backgrounds. Given the functional importance of the CUT homeodomain binding site in the *rab-3* locus described above, we were surprised to observe no *rab-3/RAB3* expression defects in either single or *ceh-44*; *ceh-48* double null mutant animals (Figure 3A).

ChIP analysis from the modENCODE project shows that the conserved and ubiquitously expressed CEH-38 ONECUT protein displays the same binding profile to pan-neuronal genes as the CEH-48 protein does²¹ (Figures 2A and S2; Data S1A–S1C). Moreover, motif extraction from the ChIP-seq data reveals that CEH-48 and CEH-38 consensus binding motifs are identical (Figure 2A). To test the possibility that CEH-38 could compensate for the loss of *ceh-44* and *ceh-48*, we generated a triple *ceh-44*; *ceh-48*; *ceh-38* null mutant strain and indeed observed a reduction of *rab-3/RAB3* expression (Figure 3A). Since *rab-3/RAB3* expression was reduced, but not eliminated, and the

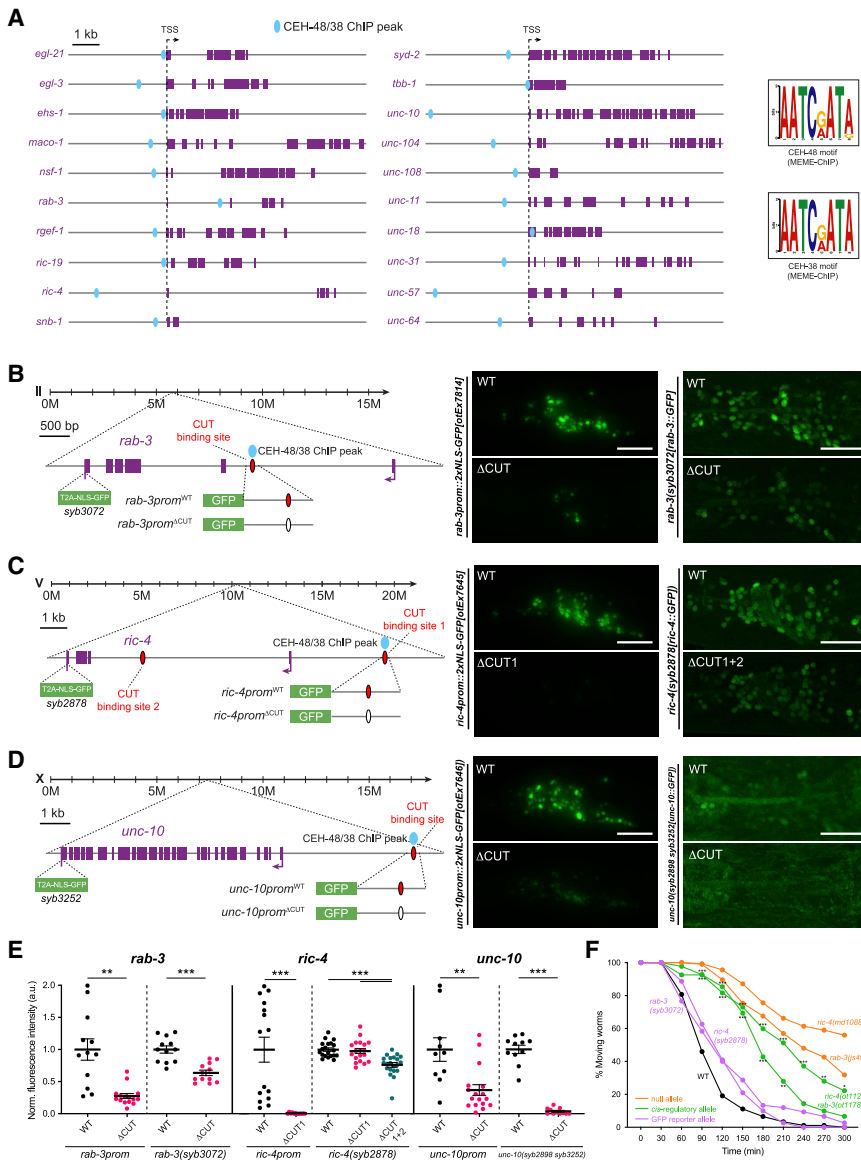


Figure 2. CUT gene binding is required for pan-neuronal gene expression

(A) Schematic representation of 20 pan-neuronal genes and the location of CEH-48 and CEH-38 peaks found in the ChIP-seq datasets. CEH-48 and CEH-38 peaks overlap for all genes except in *maco-1* and *tbb-1*, which only contain CEH-38 peaks, and *ric-19*, which only contains a CEH-48 peak. Scale represents 2 kb for *unc-104* and *unc-31*. The consensus binding motifs for CEH-48 and CEH-38, extracted from the ChIP-seq datasets using MEME-ChIP,¹⁷ are shown on the right. See [Data S1A–S1C](#) for a full list of genes with CEH-48 and CEH-38 ChIP peaks. See [Figure S2](#) for how CUT ChIP binding correlates with the *cis*-regulatory elements that we previously defined in pan-neuronally expressed genes.⁴

(B–D) Schematic representation of *rab-3* (B), *ric-4* (C), and *unc-10* (D) gene loci (left) showing the location of CEH-48/CEH-38 ChIP peaks, CUT homeodomain binding sites, endogenous GFP tags for CRISPR reporters *rab-3*(*syb3072* [*rab-3::T2A::3xNLS::GFP*]), *ric-4*(*syb2878*[*ric-4::T2A::3xNLS::GFP*]), *unc-10*(*syb2898 syb3252*[*unc-10::T2A::3xNLS::GFP*]), and small promoters tested (*rab-3prom10::2xNLS-GFP*[*otEx7814*], *ric-4prom30::2xNLS-GFP*[*otEx7645*], and *unc-10prom12::2xNLS-GFP*[*otEx7646*]). Blue ovals indicate binding based on ChIP-seq peak data and red ovals indicate binding site based on sequence. Worm head GFP images showing a reduction in pan-neuronal gene expression when the CUT homeodomain binding site is mutated compared with WT (middle, left). Mutation of the same CUT homeodomain binding sites endogenously in the context of CRISPR reporters affects pan-neuronal expression (middle, right). *ric-4* *gfp*-tagged allele expression is only affected upon mutation of additional CUT homeodomain binding sites (sites 1 and 2). *unc-10* *gfp*-tagged allele expression is very dim, and expression is not visible in all neurons. All images correspond to worms at the L4 larval stage. (E) Quantification of small promoter and CRISPR reporter (shown in B–D) head neuron fluorescence intensity in wild type and upon CUT homeodomain binding site mutations in the regulatory control regions of *rab-3* (left), *ric-4* (center), and *unc-10* (right). Each dot represents the expression level within one worm with the mean \pm SEM indicated. Unpaired t test, ***p* < 0.01, ****p* < 0.001. For *ric-4*(*syb2878* [*ric-4::T2A::3xNLS::GFP*]), one-way ANOVA followed by Tukey’s multiple comparisons test; ****p* < 0.001. *n* \geq 10 for all genotypes.

(F) Aldicarb-sensitivity defects in wild-type animals, *ric-4* and *rab-3* CRISPR reporter alleles (*rab-3*(*syb3072*), *ric-4*(*syb2878*)), *ric-4* and *rab-3* *cis*-regulatory alleles (*ric-4*(*ot1123 syb2878*), *rab-3*(*ot1178 syb3072*)), and *ric-4* and *rab-3* null alleles (*ric-4*(*md1088*), *rab-3*(*js49*)). Wild-type data are represented with black dots, the CRISPR reporter alleles with purple dots, the *cis*-regulatory alleles with green dots, and null alleles with orange dots. Two-way ANOVA followed by Tukey’s multiple comparisons test; comparisons for *ric-4* and *rab-3* *cis*-regulatory alleles versus wild type indicated; **p* < 0.05, ***p* < 0.01, ****p* < 0.001. *n* \geq 3 independent experiments (25 animals per independent experiment). Mean and SEM values are provided in [Data S5A](#). TSS, transcription start site; WT, wild type; a.u., arbitrary units. Scale bar, 15 μ m for all panels, except for CRISPR reporters in (B)–(D), where scale bars equal 10 μ m.

ceh-38 result indicated that even a ubiquitously expressed CUT gene contributed to the regulation of pan-neuronal gene expression, we also considered a role of the three remaining ubiquitously expressed CUT genes, *ceh-41*, *ceh-21*, and *ceh-39*. We used CRISPR/Cas9 to generate a precise deletion of those three genes, all located in an operon on the X chromosome and found that this deletion (*otDf1*; [Figure 1D](#)) alone had no significant effect on *rab-3* reporter expression ([Figure 3A](#)). However, adding this triple gene deletion to a *ceh-44*;*ceh-48*;*ceh-38* triple mutant revealed that such sextuple CUT mutant strain displayed the

strongest effect on *rab-3* expression throughout the nervous system ([Figure 3A](#)). Sextuple CUT mutants further displayed a significant reduction in the expression of four other pan-neuronal genes, *unc-11*/*SNAP91*, *ric-19*/*ICA1*, *ric-4*/*SNAP25*, and *egl-3*/*PCSK2* ([Figures 3B–3E](#); for *unc-11*, due to linkage issues, we only generated a quintuple mutant). We tested whether two of these additional pan-neuronal genes, *unc-11*/*SNAP91* and *ric-19*/*ICA1*, show cumulative expression defects upon removal of individual and multiple CUT genes in combination and found this to be the case ([Figures 3B and 3C](#)). The joint involvement

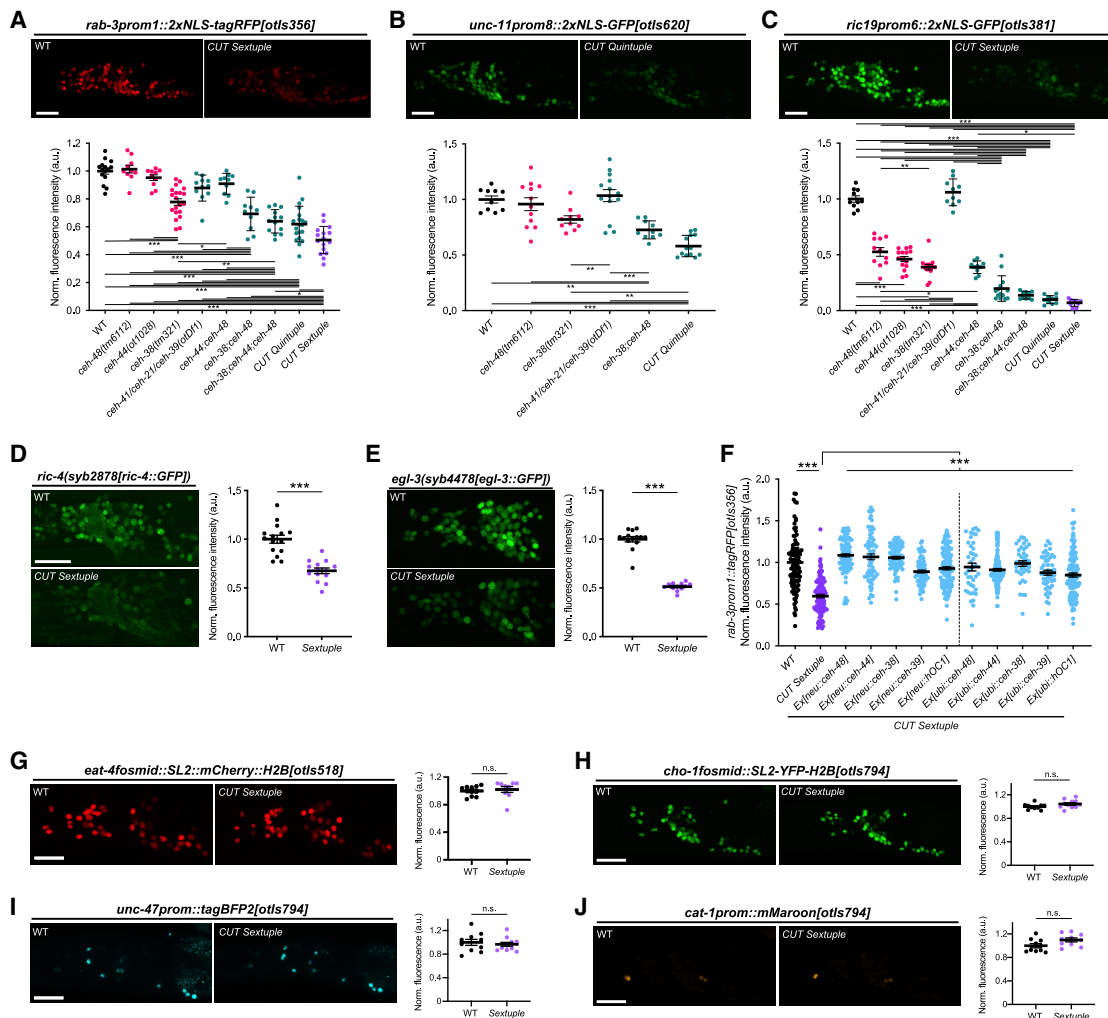


Figure 3. CUT genes act in a dosage-dependent manner to control pan-neuronal gene expression

(A–C) Expression of *rab-3prom1::2xNLS-tagRFP[otIs356]* (A), *unc-11prom8::2xGFP[otIs620]* (B), and *ric19prom6::2xNLS-GFP[otIs381]* (C) in wild type (left) and CUT sextuple mutant (right). Lateral views of the worm head at the L4 stage are shown. Quantification of fluorescence intensity in head neurons (bottom) in wild type, individual CUT mutants (*ceh-48(tm6112)*, *ceh-44(ot1028)*, and *ceh-38(tm321)*), and compound CUT mutants (*otDf1*, which deletes *ceh-41*, *ceh-21*, and *ceh-39*; double *ceh-44;ceh-48*, double *ceh-38;ceh-48*, triple *ceh-38;ceh-44;ceh-48*, quintuple *ceh-38;ceh-48;otDf1*, and sextuple *ceh-38;ceh-44;ceh-48;otDf1*). *unc-11prom8::2xGFP[otIs620]* and *ceh-44* are located in the same chromosome (chr. III) and cannot be recombined together. Each dot represents the expression level within one worm with the mean \pm SEM indicated. Wild-type data are represented with black dots, individual CUT mutants with pink dots, the sextuple CUT mutant with purple dots, and other compound CUT mutants with green dots. One-way ANOVA followed by Tukey's multiple comparisons test; * $p < 0.05$, ** $p < 0.01$, *** $p < 0.001$. $n \geq 10$ for all genotypes. All genotypes were compared, but only those comparisons that show statistically significant differences are indicated with lines.

(D and E) Expression of *ric-4(syb2878[ric-4::GFP])* (*ric-4(syb2878[ric-4::T2A-3xNLS-GFP])*) (D) and *egl-3(syb4478[egl-3::GFP])* (*egl-3(syb4478[egl-3::SL2-GFP-H2B])*) (E) in wild type (top) and CUT sextuple mutant (bottom). Lateral views of the worm head at the L4 stage are shown. Quantification of CRISPR alleles fluorescence intensity in head neurons. The data are presented as individual values with each dot representing the expression level of one worm with the mean \pm SEM indicated. Unpaired t test, *** $p < 0.001$. $n \geq 12$ for all genotypes.

(F) Expression of *rab-3prom1::2xNLS-tagRFP[otIs356]* was compared between wild type, CUT sextuple mutant, and CUT sextuple mutant rescue (pan-neuronal, *ceh-48* promoter ["neu"; see Figure S4], or ubiquitous, *eft-3* promoter ["ubi"], expression of *ceh-48*, *ceh-44*, *ceh-38*, *ceh-39*, or *hOC1*). Quantification of fluorescence intensity analyzed by COPAS system ("worm sorter"). The data are presented as individual values with each dot representing the expression level of one worm with the mean \pm SEM indicated. Wild-type data are represented with black dots, the sextuple CUT mutant with purple dots, and rescue lines with blue dots. One-way ANOVA followed by Tukey's multiple comparisons test; *** $p < 0.001$. $n \geq 40$ for all genotypes.

(G–J) Neurotransmitter reporter transgenes in CUT gene mutants. Transgenes are *otIs518* (*eat-4fosmid::SL2::mCherry::H2B*) (G) and *otIs794*, which contains *cho-1fosmid::NLS-SL2-YFP-H2B* (H), *unc-47prom::tagBFP2* (I), and *cat-1prom::mMaroon* (J), analyzed in a wild type (left) or CUT sextuple mutant background (right). Lateral views of the worm head at the L4 stage are shown. Quantification of fluorescence intensity in head neurons. Each dot represents the expression level within one worm with the mean \pm SEM indicated. $n \geq 10$ for all genotypes.

WT, wild type; a.u., arbitrary units; n.s., not significant. Scale bars, 15 μ m.

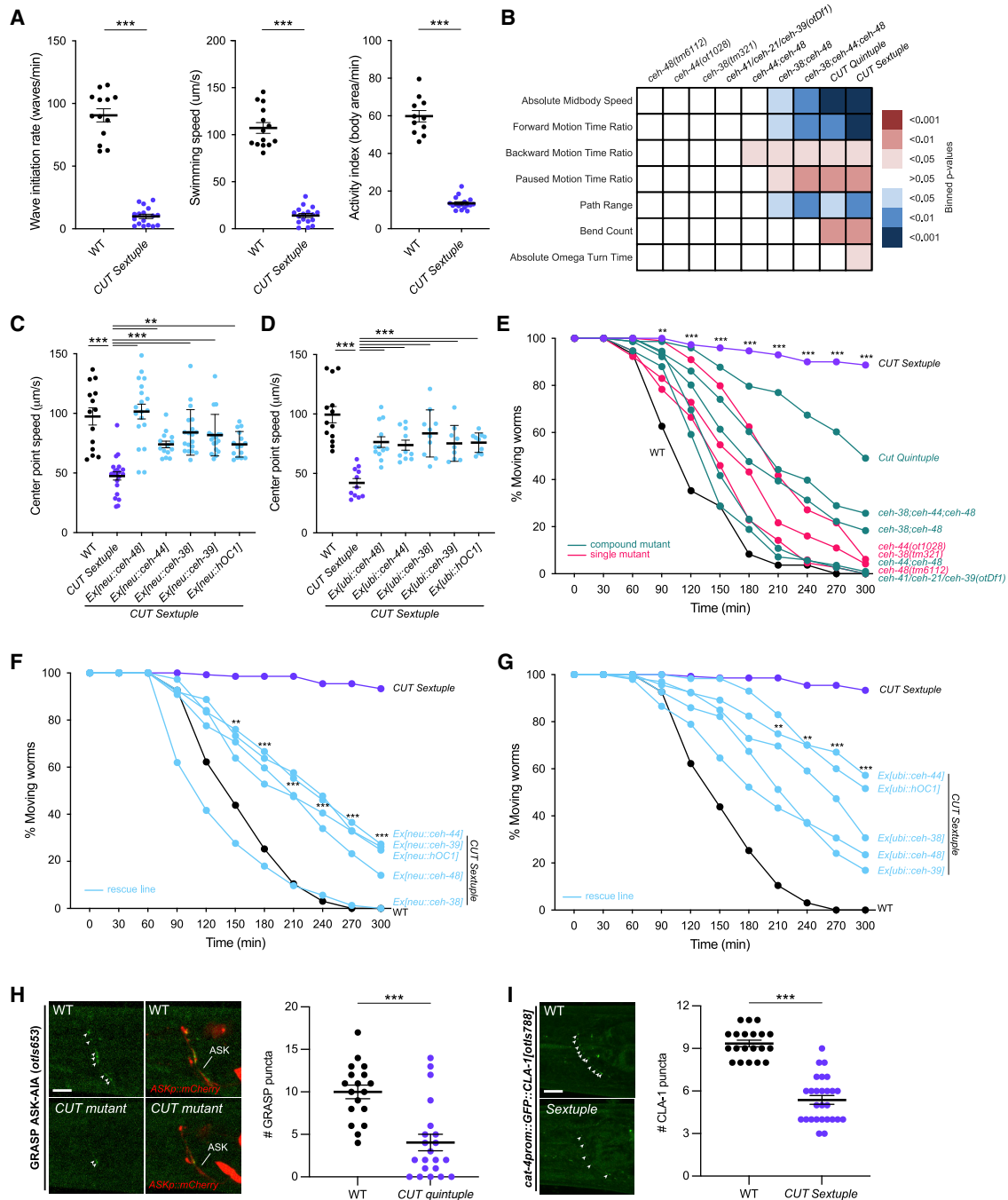


Figure 4. CUT genes are required for proper neuronal function

(A) Swimming behavior: wave initiation rate (left), swimming speed (center), and activity index (right) were compared between wild type and CUT sextuple mutant animals using a multiworm tracker system.²⁵ Each dot represents the value within one worm with the mean ± SEM indicated. Unpaired t test, ***p < 0.001. n ≥ 11 for all genotypes.

(B) Behavioral phenotypic summaries of representative locomotion features for individual and compound CUT mutants, analyzed using an automated worm tracker system.²⁶ Heat map colors indicate the p value for each feature for the comparison between each of the mutant strains and the wild-type strain. Red indicates a significant increase for the tested feature, while blue indicates a significant decrease. One-way ANOVA followed by Tukey's multiple comparisons test. n ≥ 10 for all genotypes. Time ratio = total time spent performing behavior/total assay time.

(C and D) Worm speed was compared among wild type, CUT sextuple mutant, and CUT sextuple mutant rescue (pan-neuronal, *ceh-48* promoter ["neu"; see Figure S4; C], or ubiquitous, *eft-3* promoter ["ubi"; D], expression of *ceh-48*, *ceh-44*, *ceh-38*, *ceh-39*, or *hOC1*) using a multiworm tracker system.⁴⁶ Each dot represents the expression level within one worm with the mean ± SEM indicated. Wild-type data are represented with black dots, the sextuple CUT mutant

(legend continued on next page)

of multiple CUT genes provides an explanation for why previous screens for mutants affecting pan-neuronal gene expression were unsuccessful¹² and are a testament to the robustness of pan-neuronal gene expression control.

Defects observed in the compound CUT mutants appear complementary to the gene expression defects observed in neuron-type-specific terminal selector mutants. Specifically, several exemplary genes that are more selectively expressed in the nervous system, including *cho-1/ChT* (a marker that is exclusive to cholinergic neurons), *eat-4/VGLUT* (a marker specific to glutamatergic neurons), *unc-47/VGAT* (a marker specific for GABAergic neurons), and *cat-1/VMAT* (monoaminergic neuron marker), were not affected in sextuple CUT mutant animals (Figures 3G–3J). This result is consistent with these genes lacking ChIP peaks of CUT protein binding (Data S1A–S1C). Thus, the sextuple CUT mutant phenotype appears to be a mirror image of the phenotype of terminal selector transcription factors, whose removal results in loss of neuron-type-specific identity features (such as the tested *cho-1/ChT*, *eat-4/VGLUT*, *unc-47/VGAT*, and *cat-1/VMAT*), but not pan-neuronal identity features.⁵

As expected from a loss of pan-neuronal gene expression, sextuple CUT mutant animals are severely deficient in nervous system function (Figures 4A, 4B, and 4E). Animals display an almost complete paralysis in swimming assays, a sensitive and well quantifiable readout of animal locomotion (Figure 4A).^{27–29} Crawling behavior on an agar surface, quantified using a semi-automated WormTracker system, is also severely affected in sextuple CUT mutant animals (Figure 4B). Synaptic transmission defects, scored via responsiveness to aldicarb, are also very obvious; CUT sextuple mutants display a strong resistance to aldicarb (Figure 4E). Crawling and synaptic transmission defects are again cumulative, i.e., defects worsen as more CUT genes are removed (Figures 4B and 4E). Overall nervous system

anatomy is unaffected in CUT sextuple mutants, including general cell body and fascicle position (Figure S3). However, a visualization of synaptic punctae with the active zone marker CLA-1³⁰ or with a neuroligin-based GRASP strain³¹ reveals defects in synapse abundance in compound CUT gene mutants (Figures 4H and 4I).

The cumulative effects of CUT homeobox gene removal suggest a scenario in which it is primarily the overall dosage of CUT genes, rather than specific features of each individual CUT gene that is important to specify pan-neuronal gene expression. To further test this notion, we re-introduced individual CUT genes into the sextuple CUT mutant background. We used two separate drivers—a ubiquitous driver (*eft-3prom*) or a pan-neuronal driver (a fragment from the *ceh-48* locus, *ceh-48prom4*; Figure S4A)—to generate multicopy transgenic arrays for overexpression. We found that each individually tested overexpressed *C. elegans* CUT gene is alone able to rescue (1) the pan-neuronal gene expression defects (Figure 3F) and (2) the crawling and synaptic transmission defects of sextuple mutant animals (Figures 4C, 4D, 4F, 4G, and S4B–S4E).

To assess potential phylogenetic conservation of CUT gene function, we also overexpressed a human ONECUT homolog, *hOC1*, and found that it is also capable of rescuing the *C. elegans* CUT sextuple mutant phenotype (Figures 3F, 4C, 4D, 4F, 4G, and S4B–S4E).

Taken together, these results allow us to draw four conclusions: first, the usage of the postmitotic, pan-neuronal *ceh-48* promoter indicates that CUT genes indeed act cell-autonomously in postmitotic neurons; second, CUT genes are functionally interchangeable; third, CUT gene dosage in the nervous system appears to be the main determinant of CUT gene function as regulators of pan-neuronal gene expression; and fourth, CUT gene function may be phylogenetically conserved.

with purple dots, and rescue lines with blue dots. One-way ANOVA followed by Tukey's multiple comparisons test, comparisons with CUT sextuple mutant indicated; **p < 0.01, ***p < 0.001. n ≥ 10 for all genotypes. See Figure S4 for additional locomotion features.

(E) Aldicarb-sensitivity defects in individual CUT mutants (*ceh-48(tm6112)*, *ceh-44(ot1028)*, *ceh-38(tm321)*) and compound CUT mutants (*otDf1*, which deletes *ceh-41*, *ceh-21*, and *ceh-39*; double *ceh-44*; *ceh-48*, double *ceh-38*; *ceh-48*, triple *ceh-38*; *ceh-44*;*ceh-48*, quintuple *ceh-38*; *ceh-48*; *otDf1*, and sextuple *ceh-38*; *ceh-44*; *ceh-48*; *otDf1*) compared with wild-type animals. Aldicarb is an acetylcholinesterase inhibitor that paralyzes worms. Decreased sensitivity to aldicarb correlates with a reduction in synaptic transmission.⁴⁸ Worms were tested every 30 min for paralysis by touching the head and tail three times each. The data are presented as the percentage of moving worms at the indicated time point; dots represent the mean of independent experiments for each genotype. Wild-type data are represented with black dots, individual CUT mutants with pink dots, the sextuple CUT mutant with purple dots, and other compound CUT mutants with green dots. Two-way ANOVA followed by Tukey's multiple comparisons test, comparisons for wild type versus CUT sextuple mutant indicated; **p < 0.01, ***p < 0.001. n ≥ 3 independent experiments (25 animals per independent experiment). Mean and SEM values are provided in Data S5B.

(F and G) Aldicarb-sensitivity defects in wild-type animals, CUT sextuple mutant, and CUT sextuple mutant rescue lines (pan-neuronal or ubiquitous, F and G, respectively). Wild-type data are represented with black dots, the sextuple CUT mutant with purple dots, and rescue lines with blue dots. Two-way ANOVA followed by Tukey's multiple comparisons test, comparisons for CUT sextuple mutant versus Ex[neu::ceh-44] (F), and CUT sextuple mutant versus Ex[ubi::ceh-44] (G) indicated; **p < 0.01, ***p < 0.001. n ≥ 3 independent experiments (25 animals per independent experiment). Mean and SEM values are provided in Data S5B.

(H) ASK-AIA GRASP signal for the ASK>AIA (*otIs653*) synaptic connection in wild type (top) and CUT quintuple mutant (*ceh-38(tm321)*; *ceh-44(ot1028)*; *otDf1*) (bottom). Lateral views of L1 worm heads at the nerve ring level are shown. ASK axon is labeled with cytoplasmic mCherry. Arrowheads indicate GRASP GFP synaptic puncta. *otIs653* and *ceh-48* are located in the same chromosome and cannot be recombined together. Quantification of puncta along the ASK axon in the nerve ring. The data are presented as individual values with each dot representing the number of puncta in one worm with the mean ± SEM indicated. Unpaired t test, ***p < 0.001. n ≥ 18 for all genotypes.

(I) HSN presynaptic specializations labeled by GFP-CLA-1 (*cat-4prom::GFP::CLA-1[otIs788]*) in wild type (top) and CUT sextuple mutant (bottom). Lateral views of young adult worm heads at the nerve ring level are shown. Arrowheads indicate CLA-1 presynaptic specializations. Quantification of CLA-1 puncta along the HSN axon in the nerve ring. The data are presented as individual values with each dot representing the number of puncta in one worm with the mean ± SEM indicated. Unpaired t test, ***p < 0.001. n ≥ 20 for all genotypes. See Figure S3 for overall nervous system anatomy.

WT, wild type; scale bars, 5 μm.

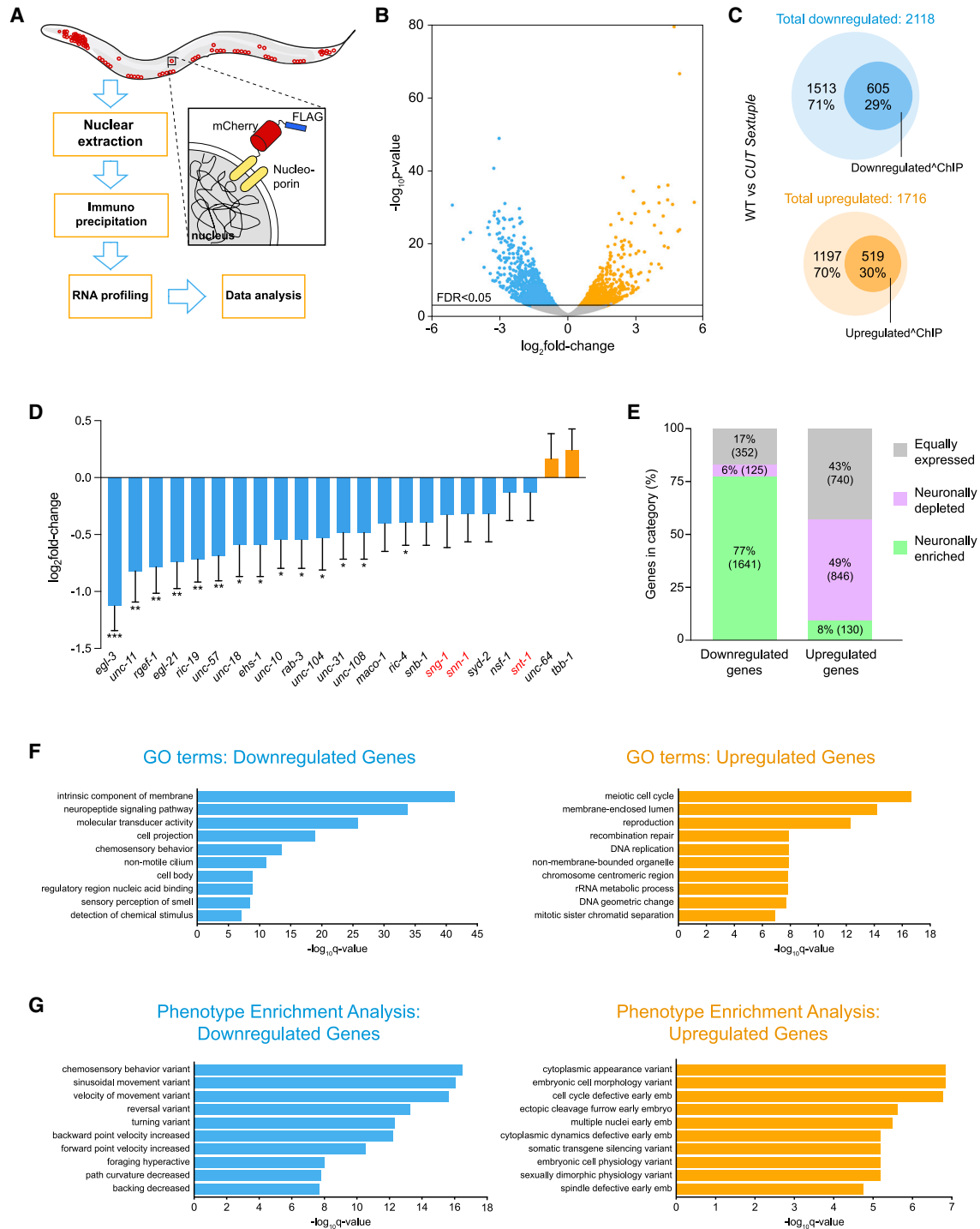


Figure 5. Transcriptional profiling of CUT sextuple mutants

(A) Schematic and experimental design for INTACT sample collection, protocol, and data analysis for neuronal transcriptome profiling.

(B) Volcano plot of differentially expressed genes in CUT sextuple mutant neurons showing significantly (FDR < 0.05) downregulated (blue) or upregulated (orange) genes (RNA-seq, n = 3). See [Data S2A](#) for the full list of differentially expressed genes.

(C) Diagrams showing the overlap between differentially expressed genes in CUT sextuple mutant and genes bound by CEH-48 or CEH-38 in a wild-type ChIP-seq.²¹ Downregulated genes are marked in blue, upregulated genes are marked in orange, and the genes that contain CUT peaks are marked with dark circles within both clusters. See [Figure S5](#) for the effect on ubiquitously expressed genes containing CUT peaks. WT, wild type.

(D) Changes of previously described pan-neuronal gene battery⁴ in CUT sextuple mutant animals. The data are presented as the log₂ fold change ± standard error calculated by DESeq2, comparing neuronal samples from wild type and CUT sextuple mutant. The two-stage step-up method of Benjamini, Krieger, and Yekutieli

(legend continued on next page)

Genome-wide analysis of CUT homeobox gene targets

We further expanded our characterization of CUT gene function by RNA transcriptome profiling of CUT gene mutant animals. To this end, we used isolation of nuclei tagged in specific cell types (INTACT) technology^{32,33} to isolate all neuronal nuclei and compared neuronal transcriptomes of wild-type animals with those of sextuple CUT mutant animals (Figure 5A). Apart from upregulated genes, we found >2,000 genes to be downregulated (FDR < 0.05) and about 605 (29%) of those have CUT homeodomain binding ChIP peaks (Figures 5B and 5C; Data S2A–S2D). Downregulated genes with CUT homeodomain binding peak include known pan-neuronally expressed genes involved in the synaptic vesicle cycle (e.g., *unc-57/SH3GL3*, *ric-19/ICA1*, and *unc-11/SNAP91*), synaptic activity zone assembly (e.g., *cla-1/PCLO*), neuronal transport (e.g., *unc-116/JIP3*), axon pathfinding (e.g., *unc-14/RUSC1*), neuronal cytoskeleton (e.g., *unc-119/UNC119* and *unc-69/SCOC*), neuropeptide processing (e.g., *egl-3/PCSK2*, *egl-21/CPE*, and *pamn-1/PAM*), and other previously known pan-neuronal genes⁴ (e.g., *rgef-1/RASGRP3*, a commonly used pan-neuronal marker). Focusing on the battery of 23 pan-neuronal genes whose expression patterns we had defined in a previous analysis,⁴ we found that most of them show reduced transcript levels in the CUT sextuple mutant (Figure 5D). As described above, we have validated these changes in the expression for *rab-3*, *unc-11*, *ric-19*, *ric-4*, and *egl-3* (Figures 3A–3E).

The use of INTACT technology to isolate the entire nervous system from wild-type animals identifies 6,372 neuronally enriched genes through comparison of neuronal nuclei to total nuclei samples (Figure 5E; Data S3A and S3B). Among the differentially expressed genes in CUT sextuple mutants, a large proportion (77%) of the downregulated gene set corresponds to this neuronally enriched gene set, while only 8% of the upregulated genes belong to the neuronally enriched gene set. Around half of the upregulated genes are actually neuronally depleted genes, whereas the other half corresponds to genes equally distributed between the nervous system and the whole animal (Figure 5E; Data S3A–S3C). Moreover, the downregulated gene set, but not the upregulated set, displays significantly GO term enrichment for several neuronal processes (e.g., neuropeptide signaling pathway, chemosensory behavior) (Figure 5F; Data S4A and S4B). Similarly, phenotype enrichment analysis for the downregulated, but not upregulated gene set, shows a large amount of locomotion phenotypes (Figure 5G; Data S4C and S4D). These findings are consistent with our reporter gene analysis, as well as our behavioral analysis, confirming that CUT homeodomain proteins are critical activators of pan-neuronal genes essential for proper neuronal function.

We find that the expression of some ubiquitously expressed genes, with potential selective functions in the nervous system,

can also be CUT gene dependent. For example, we find that the *C. elegans* orthologs of the vertebrate neuronal splicing regulator *NOVA1*,³⁴ the *C. elegans* ortholog of the alternative splicing factor *RBM25*, and the *C. elegans* homolog of a regulator of endocytosis, *EPS15*,³⁵ show diminished transcript levels in the transcriptome analysis of CUT sextuple mutants. All three loci show binding of CUT proteins by ChIP analysis in the modENCODE dataset (Data S1A–S1C). *gfp* reporter alleles that we generated using CRISPR/Cas9-genome engineering revealed ubiquitous expression of *nova-1/NOVA1*, *rbm-25/RBM25*, and *ehs-1/EPS15* throughout all tissue types (Figures S5A–S5C). We confirmed the CUT dependence of these genes in a number of different manners. First, we crossed the *nova-1* reporter allele into a CUT sextuple mutant background and found diminished expression in the nervous system. Second, we deleted the CUT homeodomain binding site from *nova-1* gene locus and also observed diminished expression in the nervous system (Figure S5E). Similarly, a deletion of the CUT homeodomain binding site from the ubiquitously expressed *ehs-1* gene locus also resulted in diminished neuronal expression (Figure S5D). In the case of *ehs-1*, this downregulation was specific to the nervous system since non-neuronal cells did not show downregulation (Figure S5D). Taken together, these results demonstrate the critical role of CUT-dependent gene expression of even ubiquitously expressed genes.

Finally, we used the CUT-dependent transcriptome dataset to identify novel pan-neuronally expressed genes. Due to its uncommon primary sequence, we honed in on a small, 76-amino-acid-long protein, Y44A6D.2, with no predicted signal sequence, which (1) is downregulated in CUT sextuple mutants (Data S2A–S2D) and (2) displays binding of CUT proteins in the modENCODE ChIP dataset (Data S1A–S1C). We used CRISPR/Cas9 to engineer *gfp* coding sequences at the 3' end of the gene and found that the resulting fusion protein is cytoplasmically expressed in all neurons throughout the nervous system but in no other tissue types (Figure S6). We named this locus *tpn-1* for “tiny pan-neuronal protein.” Hence, the CUT-dependent transcriptome indeed identifies, as expected, novel pan-neuronal genes.

Collaboration of CUT homeobox genes with terminal selectors

One notable feature of our CUT gene mutant analysis is that even in the sextuple CUT mutant, pan-neuronal gene expression is not uniformly eliminated. Nor do sextuple mutants display the larval lethality observed upon genetic removal of synaptic transmission machinery.³⁶ To address the apparently incomplete nature of these phenotypes, we considered our previous functional analysis of neuron-type-specific terminal selectors, which are required for the initiation of neuron-type-specific gene expression profiles.^{1,4,5,7}

(FDR 10%) was used to calculate the q values for this subset of genes, analyzing the individual p values obtained from the DESeq2 comparison. *q < 0.05, **q < 0.01, and ***q < 0.001 (RNA-seq, n = 3). All these genes show binding of CUT proteins by ChIP analysis, except those with gene name in red (Data S1A–S1C). (E) Vertical slices representation of the distribution (in percentage) of the downregulated and the upregulated gene sets between the neuronally enriched (green), neuronally depleted (purple), and equally expressed (gray) gene sets. See Data S3A–S3C for the full list of neuronally enriched and depleted genes. See Figure S6 for the validation of pan-neuronal expression of a neuronally enriched CUT gene target. (F and G) GO enrichment analysis (F) and phenotype enrichment analysis (G) using gene sets of significantly downregulated (blue) or upregulated (orange) transcripts. Graphs illustrate the 10 most significant terms. Analysis was performed using the gene set enrichment analysis tool from WormBase. See Data S4A–S4D for the full list of enriched terms.

While terminal selector removal alone does not generally affect pan-neuronal gene expression, we had found that pan-neuronal genes do contain terminal selector binding sites, and we had shown that these binding sites are functionally relevant, but only in the context of isolated *cis*-regulatory elements.⁴ Based on these findings, we had suggested that terminal selectors may provide redundant regulatory input into pan-neuronal gene expression (Figure 6A).⁴ Hence, an explanation for the lack of a complete loss of pan-neuronal gene expression in CUT sextuple mutants would be that terminal selectors are responsible for residual pan-neuronal gene expression.

We addressed this possibility by generating different septuple null mutant strains in which we jointly removed all six CUT genes together with different terminal selectors that were previously found to regulate distinct neuron-type-specific gene batteries. We indeed found that joint removal of terminal selectors and CUT genes strongly enhanced the reduction of pan-neuronal gene expression. For example, pan-neuronal gene expression in CUT sextuple mutants in ALM/PLM, HSN, BDU, and NSM is further reduced, if not completely eliminated, upon CRISPR/Cas9-mediated deletion of the POU homeobox gene *unc-86*, which is a terminal selector of these neuron classes³⁷ (Figures 6B–6F). Similarly, the CUT sextuple effect in the PVC, PHA, and PHB tail neurons is enhanced upon CRISPR/Cas9-mediated deletion of the LIM homeobox gene *ceh-14*, the terminal selector of PVC, PHA, and PHB (Figure 6G).^{38–40} Likewise, the DD and VD GABAergic motor neurons of the ventral nerve cord, which lose neuron-type-specific identity features, but not pan-neuronal identity features, upon removal of the *unc-30* Pitx homeobox gene,^{41,42} show a further reduction of pan-neuronal gene expression in a septuple CUT; *unc-30* mutant background, compared with the CUT sextuple or *unc-30* single mutant background alone (Figure 6H).

As an independent approach to removal of a terminal selector-encoding locus, we also mutated terminal selector binding sites in a pan-neuronal gene locus and asked whether this would enhance the effect of removal of CUT genes. Indeed, mutating binding sites for terminal selectors for ventral nerve cord motor neurons into a *gfp*-tagged *ric-4/SNAP25* locus further decreased *ric-4/SNAP25* expression in a CUT sextuple null mutant background (Figure 6I). These results indicate that CUT factors act in concert with terminal selectors to control pan-neuronal gene batteries.

DISCUSSION

We have shown here how a critical but previously little understood component of neuronal gene expression programs—the expression of pan-neuronal gene batteries—is controlled. We identified an entire family of transcription factors, the CUT homeodomain transcription factors, as key regulators of pan-neuronal gene expression. CUT homeobox genes are also candidate regulators of pan-neuronal gene expression in other organisms. *Drosophila*, sea urchin, and the simple chordate *Ciona* contain a single ONECUT gene with strikingly restricted pan-neuronal gene expression.^{43–45} In vertebrates, CUX and ONECUT gene numbers have expanded and display complex expression patterns within and outside the nervous system.^{46,47} Encouragingly, a recent analysis of *Ciona* ONECUT revealed changes in gene

expression of synaptic transmission molecules upon manipulation of ONECUT function in photoreceptor differentiation.⁴⁸ Another recent study revealed that ONECUT proteins can indeed induce neuronal features in a fibroblast-to-neuronal reprogramming approach *in vitro*.⁴⁹ Vertebrate ONECUT and CUX homologs are expressed in the nervous system,^{46,47} but a systematic, comparative, and side-by-side analysis of all family members remains to be conducted to assess how broadly all family members cover the entire nervous system. Our finding that a vertebrate ONECUT protein, human OC1, can rescue the CUT sextuple mutant phenotype provides an encouraging hint that vertebrate CUT proteins may similarly be involved in pan-neuronal gene regulation. Our genetic loss-of-function analysis predicts that compound mutants may need to be generated in mice to assess CUT family function in vertebrate pan-neuronal gene expression.

The identification of CUT genes as regulators of pan-neuronal genes in *C. elegans* provides a complement to the much better-understood regulation of neuron-type-specific gene batteries. Pan-neuronal genes require at least two distinct sets of direct regulatory inputs to initiate (and presumably also maintain) their expression: a proper dosage of broadly expressed CUT homeobox genes and neuron-type-specific terminal selector transcription factors (Figure 6A). Only the cumulative removal of all these regulatory inputs results in strong disruptions of pan-neuronal gene expression, illustrating a striking robustness of pan-neuronal gene regulation. The multitude of regulatory inputs into pan-neuronal gene loci that we define here by a genetic analysis of trans-acting factors predict that the *cis*-regulatory control regions of pan-neuronal gene loci are very complex, combining inputs from CUT genes, in addition to whatever type of terminal selector transcription factor a given neuron type employs. Our previous dissection of *cis*-regulatory regions of pan-neuronal gene corroborates this notion by describing a striking complexity of regulatory inputs⁴ and therefore providing a satisfying complement to our present analysis of trans-acting factors.

The robustness of pan-neuronal gene regulatory architecture contrasts with the regulation of neuron-type-specific gene batteries, where removal of individual *cis*-regulatory elements, or individual terminal selector transcription factors that act through such *cis*-regulatory elements, completely eliminates expression of neuron-type-specific genes.^{4,5} These dichotomous regulatory strategies may speak to (1) the evolvability of neuron-type-specific gene expression programs and (2) the evolutionary stability of pan-neuronal gene batteries. Brain evolution involves an increase in neuronal cell-type diversity and is essentially a “variation on a theme” process, characterized by an increase in neuronal cell-type diversity in which certain parameters remain stable (pan-neuronal identity), while others rapidly evolve. The two distinct regulatory strategies for neuron-type-specific and pan-neuronal gene expression may lie at the basis of such evolutionary plasticity and stability.

Our studies underscore the centrality of homeobox genes in controlling multiple aspects of neuronal identity, not only just in terms of conferring neuron-type-specific features as has been shown before,^{13,50} but also in broadly defining what distinguishes non-neuronal from neuronal cells, a cell type that has gained the ability to communicate with others via a shared

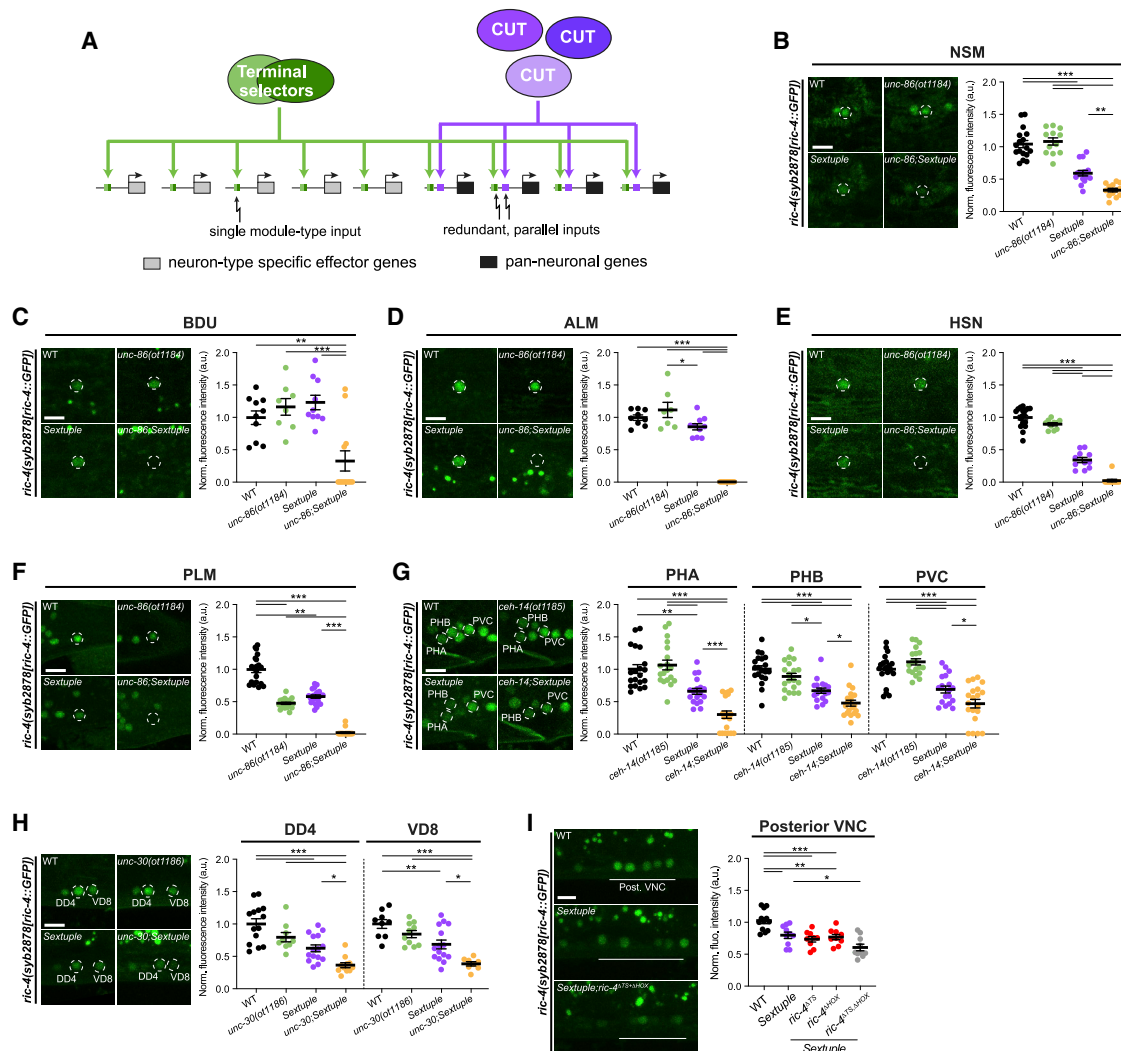


Figure 6. CUT genes cooperate with terminal selectors to control pan-neuronal gene expression

(A) Illustration for how terminal selectors contribute to the regulation of pan-neuronal gene expression.

(B–H) Expression of *ric-4(syb2878[ric-4::GFP])* (*ric-4(syb2878[ric-4::T2A-3xNLS-GFP])*) in wild type (top left), terminal selector mutant (*unc-86(ot1184)*, B–F; *ceh-14(ot1185)*, G; or *unc-30(ot1186)*, H) (top right), CUT sextuple mutant (bottom left), and compound terminal selector and CUT sextuple mutant animals (bottom right). Lateral views of the head (B), midbody (C–E and H), and tail (F and G) are shown. All images correspond to worms at the L4 larval stage, except for HSN (E) where young adults are shown. Quantification of *ric-4(syb2878[ric-4::T2A-3xNLS-GFP])* fluorescence intensity in individual neurons. Each dot represents the expression level of NSM (B), BDU (C), ALM (D), HSN (E), PLM (F), PHA, PHB, PVC (G), DD4, or VD8 (H) neuron in an individual worm, with the mean \pm SEM indicated. Wild-type data are represented with black dots, terminal selector mutants with green dots, the sextuple CUT mutant with purple dots, and compound terminal selector and CUT sextuple mutant with yellow dots. One-way ANOVA followed by Tukey's multiple comparisons test; * $p < 0.05$, ** $p < 0.01$, *** $p < 0.001$. $n \geq 8$ for all genotypes.

(I) Expression of *ric-4(syb2878[ric-4::T2A-3xNLS-GFP])* in wild type (top), CUT sextuple mutant (middle), and upon mutation of HOX and terminal selector binding sites on the *ric-4* endogenous locus in a CUT sextuple mutant background (bottom). Individual mutation of the HOX (*ric-4(ot1182 syb2878)*) or terminal selector binding sites (*ric-4(ot1181 syb2878)*) has no effect on *ric-4(syb2878[ric-4::T2A-3xNLS-GFP])* expression, but the expression is reduced in posterior ventral nerve cord (VNC) neurons when binding site mutations are combined (*ric-4(ot1183 ot1181 syb2878)*). Lateral views of the posterior VNC in L4 worms are shown. Quantification of *ric-4(syb2878[ric-4::T2A-3xNLS-GFP])* fluorescence intensity in posterior VNC neurons. Each dot represents the expression level within one worm with the mean \pm SEM indicated. Wild-type data are represented with black dots, the sextuple CUT mutant with purple dots, the sextuple mutant with individual binding sites mutated with red dots, and the sextuple mutant with both binding sites mutated with gray dots. One-way ANOVA followed by Tukey's multiple comparisons test; * $p < 0.05$, ** $p < 0.01$, *** $p < 0.001$. $n \geq 9$ for all genotypes. WT, wild type; a.u., arbitrary units. Scale bars, 5 μ m.

synaptic machinery and neuropeptides. These points indicate that the homeobox gene family may have been recruited into the control of neuronal gene expression very early in the evolution of nervous systems.

STAR★METHODS

Detailed methods are provided in the online version of this paper and include the following:

- **KEY RESOURCES TABLE**
- **RESOURCE AVAILABILITY**
 - Lead contact
 - Materials availability
 - Data and code availability
- **EXPERIMENTAL MODEL AND SUBJECT DETAILS**
 - *Caenorhabditis elegans* strains and handling
- **METHOD DETAILS**
 - CRISPR/Cas9-based genome engineering
 - Reporter transgenes
 - Automated worm tracking
 - Swimming analysis
 - Aldicarb assays
 - Microscopy
 - INTACT for purification of affinity-tagged neuronal nuclei
 - RNA-seq and data analysis
 - ChIP-seq datasets analysis
- **QUANTIFICATION AND STATISTICAL ANALYSIS**

SUPPLEMENTAL INFORMATION

Supplemental information can be found online at <https://doi.org/10.1016/j.cub.2022.02.040>.

ACKNOWLEDGMENTS

We thank Chi Chen for generating transgenic lines; HaoSheng Sun for help with the INTACT protocol; Peri Kushan for CLA-1 constructs; Maryam Majeed for providing the HSN CLA-1 and GRASP ASK-AIA strains and for help with the analysis of GRASP data; Eviatar Yemini for help with worm tracking; Cyril Cros and Molly Reilly for providing the neurotransmitter strain; Berta Vidal for providing the *rab-3* cytoplasmic strain; Waleed Ali, Kevin Gonzalez, and Mayeesa Rahman for genotyping and strain maintenance; Hynek Wichterle, Wes Gruber, Esteban Mazzoni, and members of the Hobert lab for comments on this manuscript; and WormBase and CGC (funded by NIH Office of Research Infrastructure Programs, P40 OD010440) for providing resources and reagents. This work was funded by the Howard Hughes Medical Institute and the National Institutes of Health (R01 NS 039996). E.L.-D. was supported by an EMBO long-term fellowship (ALTF 962-2014).

AUTHOR CONTRIBUTIONS

E.L.-D. and O.H. conceived the project and designed the experiments. E.L.-D. performed the experiments, imaging, and quantifications. The manuscript was prepared by E.L.-D. and O.H.

DECLARATION OF INTERESTS

The authors declare no competing interests.

Received: December 23, 2021

Revised: February 4, 2022

Accepted: February 10, 2022

Published: March 7, 2022

REFERENCES

1. Hobert, O., Carrera, I., and Stefanakis, N. (2010). The molecular and gene regulatory signature of a neuron. *Trends Neurosci.* **33**, 435–445.
2. Bürglin, T.R., and Cassata, G. (2002). Loss and gain of domains during evolution of cut superclass homeobox genes. *Int. J. Dev. Biol.* **46**, 115–123.
3. Taylor, S.R., Santpere, G., Weinreb, A., Barrett, A., Reilly, M.B., Xu, C., Varol, E., Oikonomou, P., Glenwinkel, L., McWhirter, R., et al. (2021). Molecular topography of an entire nervous system. *Cell* **184**, 4329–4347.e23.
4. Stefanakis, N., Carrera, I., and Hobert, O. (2015). Regulatory logic of pan-neuronal gene expression in *C. elegans*. *Neuron* **87**, 733–750.
5. Hobert, O. (2016). Terminal selectors of neuronal identity. *Curr. Top. Dev. Biol.* **116**, 455–475.
6. Qiu, Z., and Ghosh, A. (2008). A brief history of neuronal gene expression: regulatory mechanisms and cellular consequences. *Neuron* **60**, 449–455.
7. Hobert, O., and Kratsios, P. (2019). Neuronal identity control by terminal selectors in worms, flies, and chordates. *Curr. Opin. Neurobiol.* **56**, 97–105.
8. Bertrand, N., Castro, D.S., and Guillemot, F. (2002). Proneural genes and the specification of neural cell types. *Nat. Rev. Neurosci.* **3**, 517–530.
9. Kratsios, P., Stolfi, A., Levine, M., and Hobert, O. (2011). Coordinated regulation of cholinergic motor neuron traits through a conserved terminal selector gene. *Nat. Neurosci.* **15**, 205–214.
10. Altun-Gultekin, Z., Andachi, Y., Tsalik, E.L., Pilgrim, D., Kohara, Y., and Hobert, O. (2001). A regulatory cascade of three homeobox genes, *ceh-10*, *ttx-3* and *ceh-23*, controls cell fate specification of a defined interneuron class in *C. elegans*. *Development* **128**, 1951–1969.
11. Dykes, I.M., Tempest, L., Lee, S.I., and Turner, E.E. (2011). *Brn3a* and *Isl1* act epistatically to regulate the gene expression program of sensory differentiation. *J. Neurosci.* **31**, 9789–9799.
12. Leyva-Díaz, E., Stefanakis, N., Carrera, I., Glenwinkel, L., Wang, G., Driscoll, M., and Hobert, O. (2017). Silencing of repetitive DNA is controlled by a member of an unusual *Caenorhabditis elegans* gene family. *Genetics* **207**, 529–545.
13. Reilly, M.B., Cros, C., Varol, E., Yemini, E., and Hobert, O. (2020). Unique homeobox codes delineate all the neuron classes of *C. elegans*. *Nature* **584**, 595–601.
14. Alkema, M.J., Hunter-Ensor, M., Ringstad, N., and Horvitz, H.R. (2005). Tyramine functions independently of octopamine in the *Caenorhabditis elegans* nervous system. *Neuron* **46**, 247–260.
15. Bürglin, T.R., and Affolter, M. (2016). Homeodomain proteins: an update. *Chromosoma* **125**, 497–521.
16. Jolma, A., Yan, J., Whittington, T., Toivonen, J., Nitta, K.R., Rastas, P., Morgunova, E., Enge, M., Taipale, M., Wei, G., et al. (2013). DNA-binding specificities of human transcription factors. *Cell* **152**, 327–339.
17. Machanick, P., and Bailey, T.L. (2011). MEME-ChIP: motif analysis of large DNA datasets. *Bioinformatics* **27**, 1696–1697.
18. Love, M.I., Huber, W., and Anders, S. (2014). Moderated estimation of fold change and dispersion for RNA-seq data with DESeq2. *Genome Biol.* **15**, 550.
19. Gupta, S., Stamatoyannopoulos, J.A., Bailey, T.L., and Noble, W.S. (2007). Quantifying similarity between motifs. *Genome Biol.* **8**, R24.
20. Weirauch, M.T., Yang, A., Albu, M., Cote, A.G., Montenegro-Montero, A., Drewe, P., Najafabadi, H.S., Lambert, S.A., Mann, I., Cook, K., et al. (2014). Determination and inference of eukaryotic transcription factor sequence specificity. *Cell* **158**, 1431–1443.
21. Davis, C.A., Hitz, B.C., Sloan, C.A., Chan, E.T., Davidson, J.M., Gabdank, I., Hilton, J.A., Jain, K., Baymuradov, U.K., Narayanan, A.K., et al. (2018). The encyclopedia of DNA elements (ENCODE): data portal update. *Nucleic Acids Res.* **46**, D794–D801.
22. Nguyen, M., Alfonso, A., Johnson, C.D., and Rand, J.B. (1995). *Caenorhabditis elegans* mutants resistant to inhibitors of acetylcholinesterase. *Genetics* **140**, 527–535.
23. Nonet, M.L., Staunton, J.E., Kilgard, M.P., Fergestad, T., Hartwig, E., Horvitz, H.R., Jorgensen, E.M., and Meyer, B.J. (1997). *Caenorhabditis elegans* *rab-3* mutant synapses exhibit impaired function and are partially depleted of vesicles. *J. Neurosci.* **17**, 8061–8073.

24. elegans Deletion Mutant Consortium, C. (2012). Large-scale screening for targeted knockouts in the *Caenorhabditis elegans* genome. *G3* (Bethesda) 2, 1415–1425.
25. Roussel, N., Sprenger, J., Tappan, S.J., and Glaser, J.R. (2014). Robust tracking and quantification of *C. elegans* body shape and locomotion through coiling, entanglement, and omega bends. *Worm* 3, e982437.
26. Yemini, E., Jucikas, T., Grundy, L.J., Brown, A.E., and Schafer, W.R. (2013). A database of *Caenorhabditis elegans* behavioral phenotypes. *Nat. Methods* 10, 877–879.
27. Croll, N.A. (1975). Behavioural analysis of nematode movement. *Adv. Parasitol.* 13, 71–122.
28. Pierce-Shimomura, J.T., Chen, B.L., Mun, J.J., Ho, R., Sarkis, R., and McIntire, S.L. (2008). Genetic analysis of crawling and swimming locomotory patterns in *C. elegans*. *Proc. Natl. Acad. Sci. USA* 105, 20982–20987.
29. Restif, C., Ibáñez-Ventoso, C., Vora, M.M., Guo, S., Metaxas, D., and Driscoll, M. (2014). CeleST: computer vision software for quantitative analysis of *C. elegans* swim behavior reveals novel features of locomotion. *PLOS Comput. Biol.* 10, e1003702.
30. Xuan, Z., Manning, L., Nelson, J., Richmond, J.E., Colón-Ramos, D.A., Shen, K., and Kurshan, P.T. (2017). Clarinet (CLA-1), a novel active zone protein required for synaptic vesicle clustering and release. *eLife* 6, e29276.
31. Feinberg, E.H., Vanhoven, M.K., Bendesky, A., Wang, G., Fetter, R.D., Shen, K., and Bargmann, C.I. (2008). GFP Reconstitution Across Synaptic Partners (GRASP) defines cell contacts and synapses in living nervous systems. *Neuron* 57, 353–363.
32. Steiner, F.A., Talbert, P.B., Kasinathan, S., Deal, R.B., and Henikoff, S. (2012). Cell-type-specific nuclei purification from whole animals for genome-wide expression and chromatin profiling. *Genome Res.* 22, 766–777.
33. Sun, H., and Hobert, O. (2021). Temporal transitions in the post-mitotic nervous system of *Caenorhabditis elegans*. *Nature* 600, 93–99.
34. Jensen, K.B., Dredge, B.K., Stefani, G., Zhong, R., Buckanovich, R.J., Okano, H.J., Yang, Y.Y., and Darnell, R.B. (2000). Nova-1 regulates neuron-specific alternative splicing and is essential for neuronal viability. *Neuron* 25, 359–371.
35. Ioannou, M.S., and Marat, A.L. (2012). The role of EHD proteins at the neuronal synapse. *Sci. Signal.* 5, jc1.
36. Kohn, R.E., Duerr, J.S., McManus, J.R., Duke, A., Rakow, T.L., Maruyama, H., Moulder, G., Maruyama, I.N., Barstead, R.J., and Rand, J.B. (2000). Expression of multiple UNC-13 proteins in the *Caenorhabditis elegans* nervous system. *Mol. Biol. Cell* 11, 3441–3452.
37. Leyva-Díaz, E., Masoudi, N., Serrano-Saiz, E., Glenwinkel, L., and Hobert, O. (2020). Brn3/POU-IV-type POU homeobox genes-paradigmatic regulators of neuronal identity across phylogeny. *Wiley Interdiscip. Rev. Dev. Biol.* 9, e374.
38. Serrano-Saiz, E., Poole, R.J., Felton, T., Zhang, F., De La Cruz, E.D., and Hobert, O. (2013). Modular control of glutamatergic neuronal identity in *C. elegans* by distinct homeodomain proteins. *Cell* 155, 659–673.
39. Pereira, L., Kratsios, P., Serrano-Saiz, E., Sheftel, H., Mayo, A.E., Hall, D.H., White, J.G., LeBoeuf, B., Garcia, L.R., Alon, U., et al. (2015). A cellular and regulatory map of the cholinergic nervous system of *C. elegans*. *eLife* 4, e12432.
40. Kagoshima, H., Cassata, G., Tong, Y.G., Pujol, N., Niklaus, G., and Bürglin, T.R. (2013). The LIM homeobox gene *ceh-14* is required for phasmid function and neurite outgrowth. *Dev. Biol.* 380, 314–323.
41. Cinar, H., Keles, S., and Jin, Y. (2005). Expression profiling of GABAergic motor neurons in *Caenorhabditis elegans*. *Curr. Biol.* 15, 340–346.
42. Yu, B., Wang, X., Wei, S., Fu, T., Dzakah, E.E., Waqas, A., Walthall, W.W., and Shan, G. (2017). Convergent transcriptional programs regulate cAMP levels in *C. elegans* GABAergic motor neurons. *Dev. Cell* 43, 212–226.e7.
43. Lowe, E.K., and Stolfi, A. (2018). Developmental system drift in motor ganglion patterning between distantly related tunicates. *EvoDevo* 9, 18.
44. Nguyen, D.N.T., Rohrbaugh, M., and Lai, Z. (2000). The *Drosophila* homolog of *Onecut* homeodomain proteins is a neural-specific transcriptional activator with a potential role in regulating neural differentiation. *Mech. Dev.* 97, 57–72.
45. Poustka, A.J., Kühn, A., Radosavljevic, V., Wellenreuther, R., Lehrach, H., and Panopoulou, G. (2004). On the origin of the chordate central nervous system: expression of *Onecut* in the sea urchin embryo. *Evol. Dev.* 6, 227–236.
46. Kropp, P.A., and Gannon, M. (2016). *Onecut* transcription factors in development and disease. *Trends Dev. Biol.* 9, 43–57.
47. Weiss, L.A., and Nieto, M. (2019). The crux of *Cux* genes in neuronal function and plasticity. *Brain Res.* 1705, 32–42.
48. Vassalli, Q.A., Colantuono, C., Nittoli, V., Ferraioli, A., Fasano, G., Berruto, F., Chiusano, M.L., Kelsh, R.N., Sordino, P., and Locascio, A. (2021). *Onecut* regulates core components of the molecular machinery for neurotransmission in photoreceptor differentiation. *Front. Cell Dev. Biol.* 9, 602450.
49. van der Raadt, J., van Gestel, S.H.C., Nadif Kasri, N., and Albers, C.A. (2019). *ONECUT* transcription factors induce neuronal characteristics and remodel chromatin accessibility. *Nucleic Acids Res* 47, 5587–5602.
50. Hobert, O. (2021). Homeobox genes and the specification of neuronal identity. *Nat. Rev. Neurosci.* 22, 627–636.
51. Mahoney, T.R., Luo, S., and Nonet, M.L. (2006). Analysis of synaptic transmission in *Caenorhabditis elegans* using an aldicarb-sensitivity assay. *Nat. Protoc.* 1, 1772–1777.
52. Sarov, M., Murray, J.I., Schanze, K., Pozniakovski, A., Niu, W., Angermann, K., Hasse, S., Rupprecht, M., Vinis, E., Tinney, M., et al. (2012). A genome-scale resource for in vivo tag-based protein function exploration in *C. elegans*. *Cell* 150, 855–866.
53. Schneider, C.A., Rasband, W.S., and Eliceiri, K.W. (2012). NIH Image to ImageJ: 25 years of image analysis. *Nat. Meth.* 9, 671–675.
54. Dobin, A., Davis, C.A., Schlesinger, F., Drenkow, J., Zaleski, C., Jha, S., Batut, P., Chaisson, M., and Gingeras, T.R. (2013). STAR: ultrafast universal RNA-seq aligner. *Bioinformatics* 29, 15–21.
55. Liao, Y., Smyth, G.K., and Shi, W. (2014). featureCounts: an efficient general purpose program for assigning sequence reads to genomic features. *Bioinformatics* 30, 923–930.
56. Angeles-Albores, D., N Lee, R.Y., Chan, J., and Sternberg, P.W. (2016). Tissue enrichment analysis for *C. elegans* genomics. *BMC Bioinformatics* 17, 366.
57. Brenner, S. (1974). The genetics of *Caenorhabditis elegans*. *Genetics* 77, 71–94.
58. Dokshin, G.A., Ghanta, K.S., Piscopo, K.M., and Mello, C.C. (2018). Robust genome editing with short single-stranded and long, partially single-stranded DNA donors in *Caenorhabditis elegans*. *Genetics* 210, 781–787.
59. Hobert, O. (2002). PCR fusion-based approach to create reporter gene constructs for expression analysis in transgenic *C. elegans*. *BioTechniques* 32, 728–730.
60. Lloret-Fernández, C., Maicas, M., Mora-Martínez, C., Artacho, A., Jimeno-Martín, Á., Chirivella, L., Weinberg, P., and Flames, N. (2018). A transcription factor collective defines the HSN serotonergic neuron regulatory landscape. *eLife* 7, e32785.
61. Serrano-Saiz, E., Gulez, B., Pereira, L., Gendrel, M., Kerk, S.Y., Vidal, B., Feng, W., Wang, C., Kratsios, P., Rand, J.B., et al. (2020). Modular organization of cis-regulatory control information of neurotransmitter pathway genes in *Caenorhabditis elegans*. *Genetics* 215, 665–681.

STAR★METHODS

KEY RESOURCES TABLE

REAGENT or RESOURCE	SOURCE	IDENTIFIER
Antibodies		
Mouse monoclonal anti-FLAG M2	Sigma-Aldrich	Cat# F1804; RRID: AB_262044
Bacterial and virus strains		
<i>E. coli</i>	Caenorhabditis Genetics Center (CGC)	WormBase: OP50; WormBase: WBStrain00041969
Chemicals, peptides, and recombinant proteins		
Aldicarb	ChemService	Cat# N-11044-100MG
Sodium Azide	Sigma-Aldrich	Cat# 71289
RNase-free DMF	Acros Organics	Cat# AC327175000
OptiPrep	Cosmo Bio USA	Cat # AXS-1114542
Dynabeads Protein G	Thermo Fisher	Cat# 10003D
Dynabeads M-270 Carboxylic Acid	Thermo Fisher	Cat# 14305D
Alt-R S.p. Cas9 Nuclease V3	IDT	Cat# 1081059
Alt-R CRISPR-Cas9 tracrRNA	IDT	Cat# 1072533
Critical commercial assays		
NucleoSpin Tissue XS	Takara	Cat# 740901.250
Universal RNA-seq with NuQuant	Tecan	Cat# 0533-32
Deposited data		
Raw and analyzed RNA-seq data	This paper	GEO: GSE188489
CEH-48 ChIP-seq dataset	Davis et al. ²¹	https://www.encodeproject.org/ ; ENCODE: ENCSR844VCY
CEH-38 ChIP-seq dataset	Davis et al. ²¹	http://www.modencode.org/ ; modEncode:4800
Experimental models: Organisms/strains		
<i>C. elegans</i> : Strain N2	Caenorhabditis Genetics Center (CGC)	WormBase: N2; WormBase: WBStrain00000001
<i>ceh-38(tm321) II</i>	<i>C. elegans</i> Deletion Mutant Consortium ²⁴	FX00321
<i>ceh-48(tm6112) IV</i>	<i>C. elegans</i> Deletion Mutant Consortium ²⁴	FX06112
<i>rab-3(js49)</i>	Nonet et al. ²³	NM791
<i>otIs356(rab-3prom1::2xNLS-tagRFP) V</i>	Taylor et al. ⁴	OH10690
<i>otIs381(ric-19prom6::2xNLS-GFP) V</i>	Stefanakis et al. ⁴	OH11062
<i>otIs620(unc-11prom8::2xNLS-GFP) III</i>	Leyva-Díaz et al. ¹²	OH13606
<i>otIs518(eat-4fosmid::SL2::mCherry::H2B, pha-1(+)) V; pha-1(e2123) III</i>	Serrano-Saiz et al. ³⁸	OH13645
<i>otIs653(srg-8prom::mCherry, cho-1prom::mCherry, srg-8prom::NLG-1::spGFP1-10, cho-1prom::NLG-1::spGFP11)</i>	This study	OH15034
<i>otIs748(rab-3prom1::GFP, ttx-3prom::mCherry) X</i>	This study	OH16085
<i>otDf1 X</i>	This study	OH16103
<i>ceh-44(ot1015[ceh-44::GFP]) III</i>	Reilly et al. ¹³	OH16219
<i>ceh-49(ot1016[ceh-49::GFP]) V</i>	Reilly et al. ¹³	OH16224
<i>otEx7463(ceh-48prom4:: 2xNLS-GFP, pha-1(+)); pha-1(e2123) III</i>	This study	OH16284
<i>ceh-44(ot1028) III</i>	This study	OH16376
<i>ceh-38(tm321) II; ceh-44(ot1028) III; ceh-48(tm6112) IV; otIs356 V; otDf1 X</i>	This study	OH16377

(Continued on next page)

Continued

REAGENT or RESOURCE	SOURCE	IDENTIFIER
<i>ceh-38(tm321) II; ceh-48(tm6112) IV; otIs356 V; otDf1 X</i>	This study	OH16397
<i>ceh-38(tm321) II; ceh-48(tm6112) IV</i>	This study	OH16583
<i>ceh-44(ot1028) III; ceh-48(tm6112) IV</i>	This study	OH16584
<i>ceh-38(tm321) II; otIs356 V</i>	This study	OH16586
<i>ceh-38(tm321) II; ceh-48(tm6112) IV; otIs356 V</i>	This study	OH16587
<i>ceh-48(tm6112) IV; otIs356 V</i>	This study	OH16590
<i>ceh-38(tm321) II; ceh-44(ot1028) III; ceh-48(tm6112) IV</i>	This study	OH16593
<i>otEx7617(unc-10prom12(ΔCUT)::2xNLS-GFP, pha-1(+)); pha-1(e2123) III</i>	This study	OH16654
<i>otEx7619(rab-3prom10(ΔCUT)::2xNLS-GFP, pha-1(+)); pha-1(e2123) III</i>	This study	OH16656
<i>otEx7644(ric-4prom30(ΔCUT)::2xNLS-GFP, pha-1(+)); pha-1(e2123) III</i>	This study	OH16707
<i>otEx7645(ric-4prom30::2xNLS-GFP, pha-1(+)); pha-1(e2123) III</i>	This study	OH16708
<i>otEx7646(unc-10prom12::2xNLS-GFP, pha-1(+)); pha-1(e2123) III</i>	This study	OH16709
<i>otIs788(cat-4prom::GFP::CLA-1, cat-4prom::mCherry, inx-16prom::tagRFP)</i>	This study	OH16737
<i>otIs790(UPN::npp-9::mCherry::blpr::3xflag)</i>	Sun and Hobert ³³	OH16748
<i>otIs794(cho-1fosmid::NLS-SL2-YFP-H2B, eat-4fosmid::SL2::LSSmOrange-H2B, unc-47prom::tagBFP2, cat-1prom::mMaroon, rab3prom1::2xNLS-tagRFP)</i>	This study	OH16765
<i>ric-4(ot1123 syb2878) V</i>	This study	OH17045
<i>ceh-48(ot1125[ceh-48::GFP]) IV</i>	This study	OH17051
<i>ceh-38(tm321) II; ceh-44(ot1028) III; ceh-48(tm6112) IV; otDf1 X; otIs790(UPN::npp-9::mCherry::blpr::3xflag)</i>	This study	OH17055
<i>rab-3(ot1178 syb3072) II</i>	This study	OH17504
<i>ric-4(ot1179 ot1123 syb2878) V</i>	This study	OH17505
<i>unc-10(ot1180 syb2898 syb3252) X</i>	This study	OH17506
<i>ric-4(ot1181 syb2878) V</i>	This study	OH17507
<i>ric-4(ot1182 syb2878) V</i>	This study	OH17508
<i>ric-4(ot1183 ot1181 syb2878) V</i>	This study	OH17509
<i>ceh-38(tm321) II; ceh-44(ot1028) III; unc-86(ot1184) III; ceh-48(tm6112) IV; otDf1 X</i>	This study	OH17510
<i>ceh-38(tm321) II; ceh-44(ot1028) III; ceh-48(tm6112) IV; otDf1 X; ceh-14(ot1185) X</i>	This study	OH17511
<i>ceh-38(tm321) II; ceh-44(ot1028) III; ceh-48(tm6112) IV; unc-30(ot1186) IV; otDf1 X</i>	This study	OH17512
<i>unc-86(ot1184) III</i>	This study	OH17513
<i>ceh-14(ot1185) X</i>	This study	OH17514
<i>unc-30(ot1186) IV</i>	This study	OH17515
<i>otEx7814(rab-3prom10::2xNLS-GFP, pha-1(+)); pha-1(e2123) III</i>	This study	OH17517
<i>ceh-38(tm321) II; ceh-44(ot1028) III; ceh-48(tm6112) IV; ric-4(syb2878) V; otDf1 X</i>	This study	OH17518
<i>ceh-38(tm321) II; ceh-44(ot1028) III; ceh-48(tm6112) IV; egl-3(syb4478) V; otDf1 X</i>	This study	OH17519
<i>ceh-38(tm321) II; ceh-48(tm6112) IV; otDf1 X</i>	This study	OH17520
<i>ceh-38(tm321) II; ceh-44(ot1028) III; ceh-48(tm6112) IV; otDf1 X</i>	This study	OH17521
<i>ceh-38(tm321) II; ceh-44(ot1028) III; otDf1 X; otIs653</i>	This study	OH17522
<i>ceh-38(tm321) II; ceh-44(ot1028) III; ceh-48(tm6112) IV; otDf1 X; otIs788</i>	This study	OH17523

(Continued on next page)

Continued

REAGENT or RESOURCE	SOURCE	IDENTIFIER
<i>ceh-38(tm321) II; ceh-44(ot1028) III; ceh-48(tm6112) IV; otIs518 V; otDf1 X</i>	This study	OH17524
<i>ceh-38(tm321) II; ceh-44(ot1028) III; ceh-48(tm6112) IV; otDf1 X; otIs794</i>	This study	OH17525
<i>ceh-38(tm321) II; ceh-44(ot1028) III; ceh-48(tm6112) IV; otDf1, otIs748 X</i>	This study	OH17526
<i>otEx7815(ceh-48prom4::ceh-48, ttx-3prom::GFP); ceh-38(tm321) II; ceh-44(ot1028) III; ceh-48(tm6112) IV; otIs356 V; otDf1 X</i>	This study	OH17527
<i>otEx7816(ceh-48prom4::ceh-44, ttx-3prom::GFP); ceh-38(tm321) II; ceh-44(ot1028) III; ceh-48(tm6112) IV; otIs356 V; otDf1 X</i>	This study	OH17528
<i>otEx7817(ceh-48prom4::ceh-38, ttx-3prom::GFP); ceh-38(tm321) II; ceh-44(ot1028) III; ceh-48(tm6112) IV; otIs356 V; otDf1 X</i>	This study	OH17529
<i>otEx7818(ceh-48prom4::ceh-39, ttx-3prom::GFP); ceh-38(tm321) II; ceh-44(ot1028) III; ceh-48(tm6112) IV; otIs356 V; otDf1 X</i>	This study	OH17530
<i>otEx7819(ceh-48prom4::hOC1, ttx-3prom::GFP); ceh-38(tm321) II; ceh-44(ot1028) III; ceh-48(tm6112) IV; otIs356 V; otDf1 X</i>	This study	OH17531
<i>otEx7820(eft-3prom::ceh-48, ttx-3prom::GFP); ceh-38(tm321) II; ceh-44(ot1028) III; ceh-48(tm6112) IV; otIs356 V; otDf1 X</i>	This study	OH17532
<i>otEx7821(eft-3prom::ceh-44, ttx-3prom::GFP); ceh-38(tm321) II; ceh-44(ot1028) III; ceh-48(tm6112) IV; otIs356 V; otDf1 X</i>	This study	OH17533
<i>otEx7822(eft-3prom::ceh-38, ttx-3prom::GFP); ceh-38(tm321) II; ceh-44(ot1028) III; ceh-48(tm6112) IV; otIs356 V; otDf1 X</i>	This study	OH17534
<i>otEx7823(eft-3prom::ceh-39, ttx-3prom::GFP); ceh-38(tm321) II; ceh-44(ot1028) III; ceh-48(tm6112) IV; otIs356 V; otDf1 X</i>	This study	OH17535
<i>otEx7824(eft-3prom::hOC1, ttx-3prom::GFP); ceh-38(tm321) II; ceh-44(ot1028) III; ceh-48(tm6112) IV; otIs356 V; otDf1 X</i>	This study	OH17536
<i>ceh-44(ot1028) III; otIs356 V</i>	This study	OH17537
<i>otIs356 V; otDf1 X</i>	This study	OH17538
<i>ceh-44(ot1028) III; ceh-48(tm6112) IV; otIs356 V</i>	This study	OH17539
<i>ceh-38(tm321) II; ceh-44(ot1028) III; ceh-48(tm6112) IV; otIs356 V</i>	This study	OH17540
<i>otIs620 III; ceh-48(tm6112) IV</i>	This study	OH17541
<i>ceh-38(tm321) II; otIs620 III</i>	This study	OH17542
<i>otIs620 III; otDf1 X</i>	This study	OH17543
<i>ceh-38(tm321) II; otIs620 III; ceh-48(tm6112) IV</i>	This study	OH17544
<i>ceh-38(tm321) II; otIs620 III; ceh-48(tm6112) IV; otDf1 X</i>	This study	OH17545
<i>ceh-48(tm6112) IV; otIs381 V</i>	This study	OH17546
<i>ceh-44(ot1028) III; otIs381 V</i>	This study	OH17547
<i>ceh-38(tm321) II; otIs381 V</i>	This study	OH17548
<i>otIs381 V; otDf1 X</i>	This study	OH17549
<i>ceh-44(ot1028) III; ceh-48(tm6112) IV; otIs381 V</i>	This study	OH17550
<i>ceh-38(tm321) II; ceh-48(tm6112) IV; otIs381 V</i>	This study	OH17551
<i>ceh-38(tm321) II; ceh-44(ot1028) III; ceh-48(tm6112) IV; otIs381 V</i>	This study	OH17552
<i>ceh-38(tm321) II; ceh-48(tm6112) IV; otIs381 V; otDf1 X</i>	This study	OH17553
<i>ceh-38(tm321) II; ceh-44(ot1028) III; ceh-48(tm6112) IV; otIs381 V; otDf1 X</i>	This study	OH17554
<i>ceh-38(tm321) II; ceh-44(ot1028) III; ceh-48(tm6112) IV; nova-1(syb4373) V; otDf1 X</i>	This study	OH17584
<i>wgls241(ceh-38fosmid::TY1::EGFP::3xFLAG + unc-119(+))</i>	Sarov et al. ⁵²	OP241
<i>wgls631(ceh-48fosmid::TY1::EGFP::3xFLAG + unc-119(+))</i>	Sarov et al. ⁵²	OP631
<i>wgls759(ceh-41fosmid::TY1::EGFP::3xFLAG + unc-119(+))</i>	Sarov et al. ⁵²	OP759
<i>ric-4(syb2878[ric-4::T2A::3xNLS::GFP]) V</i>	This study	PHX2878
<i>rab-3(syb3072[rab-3::T2A::3xNLS::GFP]) II</i>	This study	PHX3072

(Continued on next page)

Continued

REAGENT or RESOURCE	SOURCE	IDENTIFIER
<i>unc-10</i> (syb2898 syb3252[<i>unc-10::T2A::3xNLS::GFP</i>]) X	This study	PHX3252
<i>nova-1</i> (syb4373[<i>nova-1::GFP</i>]) V	This study	PHX4373
<i>rbm-25</i> (syb4376[<i>rbm-25::GFP</i>]) V	This study	PHX4376
<i>ehs-1</i> (syb4426[<i>ehs-1::SL2-GFP-H2B</i>]) II	This study	PHX4426
<i>egl-3</i> (syb4478[<i>egl-3::SL2-GFP-H2B</i>]) V	This study	PHX4478
<i>ehs-1</i> (syb4426 syb4716) II	This study	PHX4716
<i>ceh-38</i> (syb4799[<i>ceh-38::GFP</i>]) II	This study	PHX4799
<i>ceh-41</i> (syb4901[<i>ceh-41::GFP</i>]) X	This study	PHX4901
<i>tpan-1</i> (syb5349[<i>tpan-1::GFP</i>]) V	This study	PHX5349
<i>nova-1</i> (syb4373 syb5446) V	This study	PHX5446
<i>ric-4</i> (md1088) V	Nguyen et al. ²²	RM956

Software and algorithms

ImageJ	Schneider et al. ⁵³	https://imagej.nih.gov/ij/
Worm Tracker v2.0	Yemini et al. ²⁶	https://www.mrc-lmb.cam.ac.uk/wormtracker/
Wormlab	Roussel et al. ²⁵	MBF Bioscience
STAR	Dobin et al. ⁵⁴	https://code.google.com/archive/p/rna-star/
featurecounts	Liao et al. ⁵⁵	http://subread.sourceforge.net/
DeSeq2	Love et al. ¹⁸	https://bioconductor.org/packages/release/bioc/html/DESeq2.html
Gene Set Enrichment Analysis tool	Angeles-Albores et al. ⁵⁶	https://wormbase.org/tools/enrichment/tea/tea.cgi
MEME-ChIP	Machanick and Bailey ¹⁷	https://meme-suite.org/meme/tools/meme-chip
Tomtom Motif Comparison Tool	Gupta et al. ¹⁹	https://meme-suite.org/meme/tools/tomtom

Other

Confocal Laser Scanning Microscope	Zeiss	LSM 880
Sequencing Platform	Illumina	NextSeq 500
Sorting Platform	Union Biometrica	COPAS FP-250
Disposable Tissue Grinder	Fisher Scientific	Cat# 02-542-09

RESOURCE AVAILABILITY

Lead contact

Further information and requests for resources and reagents should be directed to and will be fulfilled by the Lead Contact, Oliver Hobert (or38@columbia.edu).

Materials availability

All newly generated strains will be available at the *Caenorhabditis* Genetics Center (CGC).

Data and code availability

- Raw and processed RNA-seq data will be available at GEO: GSE188489.
- No original code has been generated for this paper.
- Any additional information required to reanalyze the data reported in this paper is available from the lead contact upon request.

EXPERIMENTAL MODEL AND SUBJECT DETAILS

***Caenorhabditis elegans* strains and handling**

Worms were grown at 20°C on nematode growth media (NGM) plates seeded with *E. coli* (OP50) bacteria as a food source unless otherwise mentioned. Worms were maintained according to standard protocol.⁵⁷ Wild-type strain used is Bristol variety, strain N2.

A complete list of strains and transgenes generated and used in this study is listed in the [key resources table](#). A few of the strains were previously published, and/or obtained from the CGC, the National BioResource Project (NBRP, Japan) or the Transgenome project,⁵² as detailed in the [key resources table](#).

METHOD DETAILS

CRISPR/Cas9-based genome engineering

ceh-48(*ot1125*[*ceh-48::GFP*]), *ceh-44*(*ot1028*), *otDf1*, *rab-3*(*ot1178 syb3072*), *unc-10*(*ot1180 syb2898 syb3252*), *ric-4*(*ot1123 syb2878*), *ric-4*(*ot1179 ot1123 syb2878*), *ric-4*(*ot1181 syb2878*), *ric-4*(*ot1182 syb2878*), *ric-4*(*ot1183 ot1181 syb2878*), *unc-86*(*ot1184*), *ceh-14*(*ot1185*), *unc-30*(*ot1186*) were generated using Cas9 protein, tracrRNA, and crRNAs from IDT, as previously described.⁵⁸ For *ceh-48*(*ot1125*[*ceh-48::GFP*]), one crRNA (atagattattagggtgatta) and an asymmetric double stranded *GFP-loxP-3xFLAG* cassette, amplified from a plasmid, were used to insert the fluorescent tag at the C-terminal. For *ceh-44*(*ot1028*), two crRNAs (ttaaggcgacgaagttatga and ccgaggaggcgaacagctat) and a ssODN donor (ataatatgattctataattaaggcgacgaagtatatcggcagaagaa tacgattctgaactattga) were used to delete 80 bp of *ceh-44* exon 8, introducing a frameshift in the CUT isoform of the Y54F10AM.4 locus (isoform a; the b isoform of this locus generates a different, non-homeodomain containing isoform, homologous to CASP protein²). For *otDf1*, two crRNAs (ggcacaatcttttcgaaag and atgaagaaaattatcaggat) and a ssODN donor (gaaaaggaattcg gaaatgaagaaaattatcagtcgaaaagatgatgcccgaatgttccgagaac) were used to generate a 8968 bp deletion (from position -159 upstream *ceh-39* ATG, to 89 bp downstream *ceh-41* stop codon) affecting 4 genes (deficiency, Df). The genes deleted in *otDf1* are *ceh-41*, *ceh-21*, *T26C11.9* and *ceh-39*. For *rab-3*(*ot1178 syb3072*), one crRNA (gctcacaataatggatcgat) and a ssODN donor (ctatctctcctgtagcagacgagctagcaacccaaaaaacattttgtgagcacacagagagagactcaaa) were used to mutate a CUT homeodomain binding site on *rab-3*(*syb3072*[*rab-3::T2A::3xNLS::GFP*]) CRISPR reporter (details on binding site mutations below). For *unc-10*(*ot1180 syb2898 syb3252*), one crRNA (tcgtgcttcacggaattgtg) and a ssODN donor (gcagagagagaaaagtagctgcttcacg gaattgtggagagaaaaaagatctcaagtcagagagcgcgagctctgttct) were used to mutate a CUT homeodomain binding site on *unc-10*(*syb2898 syb3252*[*unc-10::T2A::3xNLS::GFP*]) CRISPR reporter. For *ric-4*(*ot1123 syb2878*), one crRNA (atgagagccaatcgatcgt) and a ssODN donor (acgaagtgcagcagaaggaagcccgcacccacgtaaaaaaaactctcatagagagaaagagagctctctgttttct) were used to mutate a CUT homeodomain binding site ("site 1") on *ric-4*(*syb2878*[*ric-4::T2A::3xNLS::GFP*]) CRISPR reporter. For *ric-4*(*ot1179 ot1123 syb2878*), two crRNAs (gaaaaatggaagtcactgg and gggaacagagaaaagacta) and a ssODN donor (aaattcatataattccatcctcc caccaccactaaggctcatagtcgaacctataactattagt) were used to delete a 431 bp section containing 9 CUT homeodomain binding sites ("site 2") within *ric-4* intron 1, on top of *ric-4*(*ot1123 syb2878*). For *ric-4*(*ot1181 syb2878*), one crRNA (ttgacgataacagagacca) and a ssODN donor (ttgttcagctttcccaattttgtgcccaatctAAAAAAAAAAAAAAAAactctgttatcgtaaaagtgacatcttttcttctg) were used to mutate COE (UNC-3) and UNC-30 binding sites on *ric-4*(*syb2878*[*ric-4::T2A::3xNLS::GFP*]) CRISPR reporter. For *ric-4*(*ot1182 syb2878*) and *ric-4*(*ot1183 ot1181 syb2878*), one crRNA (cgaaaagagctcagcgaaaa) and a ssODN donor (tctctgctccatcattcaacaacg cttattttaaaaaaacattttcgctgagctctttctgtcttctgttctt) were used to mutate a HOX binding site on *ric-4*(*syb2878*[*ric-4::T2A::3xNLS::GFP*]) or *ric-4*(*ot1181 syb2878*). For *unc-86*(*ot1184*), two crRNAs (caaggtcccctctttcca and acaacata caatgggctacc) and a ssODN donor (tctgtctctcccagctcaaggtcccctctttacttgatcttgattgctgtttctggaac) were used to delete the entire *unc-86* locus. For *ceh-14*(*ot1185*), two crRNAs (tcttggcagtgatgagc and tgactgtggagtcagtgt) and a ssODN donor (gggacacaacattttgactctggcagtgatgcatgactccacagtacatttgaactggagaaaaaac) were used to delete the entire *ceh-14* locus. For *unc-30*(*ot1186*), two crRNAs (taagacgtaataatcctg and gtatgaaagtgaaagggc) and a ssODN donor (ccgatcactgactttgcgtaagacgg taataatcccttttcaacttactactgttcaataaacaattaa) were used to delete the entire *unc-30* locus.

rab-3(*syb3072*), *ric-4*(*syb2878*), *unc-10*(*syb2878*), *egl-3*(*syb4478*), *ceh-38*(*syb4799*), *ceh-41*(*syb4901*), *nova-1*(*syb4373*), *rbm-25*(*syb4376*), *ehs-1*(*syb4426*), *ehs-1*(*syb4426 syb4716*), *nova-1*(*syb4373 syb5446*) and *tpan-1*(*syb5349*) were generated by SUNY Biotech. *ceh-38*(*syb4799*) and *ceh-41*(*syb4901*) were generated with the exact same *GFP-loxP-3xFLAG* cassette as in *ceh-48*(*ot1125*[*ceh-48::GFP*]) for direct comparison of CUT *gfp*-tagged CRISPR alleles.

For CUT homeodomain binding site mutations, we looked for CEH-48 sites centered within the region covered by CEH-48 and/or CEH-38 ChIP peaks in *rab-3*, *ric-4*, *unc-10*, *ehs-1*, and *nova-1* regulatory regions. The CEH-48 binding motif (consensus ATCGA), is cataloged in the CIS-BP (Catalog of Inferred Sequence Binding Preferences) database (<http://cisbp.ccbp.utoronto.ca/>).²⁰ The CEH-48 motif matches known motifs for other ONECUT and CUX proteins (see [ChIP-seq datasets analysis](#) section below) (Data S6A and S6B). Deletions of CEH-48 binding sites were done by replacement of the binding site by adenines.

In *rab-3*(*syb3072*[*rab-3::T2A::3xNLS::GFP*]), ATCGAT (+2399, +2404) was mutated to AAAAAA. This site was centered within CEH-48 (+2326, +2452) and CEH-38 (+2211, +2719) ChIP peaks.

In *unc-10*(*syb2898 syb3252*[*unc-10::T2A::3xNLS::GFP*]), ATCGAT (-4558, -4553) was mutated to AAAAAA. This site was centered within CEH-48 (-4784, -4415) and CEH-38 (-4811, -4366) ChIP peaks.

In *ric-4*(*syb2878*[*ric-4::T2A::3xNLS::GFP*]), ATCGATTGG (-3683, -3675; "site 1") was mutated to AAAAAAAA. This site was centered within CEH-48 (-3832, -3598) and CEH-38 (-4062, -3521) ChIP peaks.

In *ehs-1*(*syb4426*[*ehs-1::SL2-GFP-H2B*]), ATCGAT (-220, -215) was mutated to AAAAAA. This site was centered within CEH-48 (-311, -106) and CEH-38 (-373, -168) ChIP peaks.

In *nova-1*(*syb4373*[*nova-1::GFP*]), ATCGATTTTCGAT (-1976, -1964) was mutated to AAAAAATTAATAA. This site was centered within CEH-48 (-2196, -1826) and CEH-38 (-2223, -1709) ChIP peaks.

For *ric-4*, a second set of CUT homeodomain binding sites ("site 2") was mutated within *ric-4prom25* (*cis*-regulatory element found to be broadly expressed in head neurons).⁴ A 431 bp section (+4947, +5378) in *ric-4* intron 1, containing 9 CUT homeodomain binding sites, was deleted.

The HOX/EXD motif, COE (UNC-3) motif, and UNC-30 motifs on *ric-4* were mutated following prior experiments in small *cis*-regulatory elements,⁴ but here these mutations were done on the *ric-4* CRISPR reporter allele, *ric-4(syb2878[ric-4::T2A::3xNLS::GFP])*. The HOX motif TGAATAATTG (-1064, -1055) was mutated to AAAAAAAAAA. The COE, TCCCTTGGGT (-1349, -1340), and UNC-30, TAATCC (-1352, -1347), motifs partially overlap and were mutated together: CTAATCCCTTGGGT was mutated to AAAAAA AAAAAAAAAA.

In the small *cis*-regulatory element reporters (see below) mutations in the same CUT homeodomain binding sites described here for *rab-3*, *ric-4* and *unc-10* were introduced in *rab-3prom10*, *ric-4prom30* (site 1) and *unc-10prom12*.

Reporter transgenes

The *rab-3*, *ric-4* and *unc-10* *cis*-regulatory element reporters were generated using a PCR fusion approach.⁵⁹ The *rab-3prom10* (+2326, +2452) (promoter fragment number continues the series generated for *cis*-regulatory analysis in Stefanakis et al.⁴), *ric-4prom30* (-3832, -3598) and *unc-10prom12* (-4784, -4415) promoter fragments were amplified from N2 genomic DNA and fused to *2xNLS-GFP*. These promoter fragment coordinates match those of the CEH-48 ChIP peaks in the regulatory regions of these genes. The resulting PCR fusion DNA fragments were injected as simple extrachromosomal arrays (50 ng/μL) into *pha-1(e2123)* animals, using a *pha-1* rescuing plasmid (pBX at 50 ng/μL) as co-injection marker. Extrachromosomal array lines were selected according to standard protocol. For *rab-3prom10*, *ric-4prom30* and *unc-10prom12* harboring the CUT homeodomain binding site mutations, promoters were obtained as gBlocks (IDT) and fused to *2xNLS-GFP*.

To assess neurotransmitter identity, we generated a transgene that expresses multiple reporters that assess neurotransmitter usage, including: a *cho-1* fosmid reporter construct (*cho-1fosmid::NLS-SL2-YFP-H2B*⁴), to label cholinergic neurons; an *eat-4* fosmid reporter construct (*eat-4fosmid::SL2::mCherry::H2B*,³⁸ where *mCherry* was replaced with *LSSmOrange*) to label glutamatergic neurons; *unc-47prom* (coordinates -2778, -1) fused with *TagBFP2* to label GABAergic neurons; *cat-1prom* (-1599, -1) fused with *mMaroon* to label monoaminergic neurons; and *rab-3prom1* (-1462, +2921) fused with *tagRFP* to label all neurons (pan-neuronal marker). The *cho-1fosmid::NLS-SL2-YFP-H2B* (20 ng/μL), *eat-4fosmid::SL2::LSSmOrange::H2B* (20 ng/μL), *unc-47prom::tagBFP2* (5 ng/μL), *cat-1prom::mMaroon* (5 ng/μL) and *rab3prom1::2xNLS-tagRFP* (10 ng/μL) constructs were injected together, and the resulting extrachromosomal array strain was integrated into the genome using standard UV irradiation methods. This was followed by 3 rounds of backcrossing to N2 to generate *otIs794*.

To generate *cat-4prom::GFP::CLA-1(S)* (pMM13), *cat-4prom8* (-629, -299; expressed in HSN⁶⁰) was amplified from N2 genomic DNA. The PCR fragment was cloned into PK065 (kindly shared by Peri Kurshan). *cat-4prom::mCherry* (pMM11) was generated similarly and cloned into pPD95.75. The constructs pMM13 and pMM11 were injected at 5 and 30 ng/μL, respectively, with an *inx-16prom::tagRFP* co-injection marker (10 ng/μL). The resulting extrachromosomal array strain was integrated into the genome using standard UV irradiation methods.

To label the ASK-AIA synapse with GRASP,³¹ we generated *otIs653(srg-8prom::mCherry, cho-1prom::mCherry, srg-8prom::NLG-1::spGFP1-10, cho-1prom::NLG-1::spGFP11)*. For this transgene, a 2kb *srg-8prom* (coordinates -2000, -1; expressed in ASK) was cloned into MVC2 (*pSM::NLG-1::spGFP1-10*) using RF cloning to generate *srg-8prom::NLG-1::spGFP1-10* (pMM14). *srg-8prom::mCherry* (pMM02) was generated by subcloning *srg-8prom* into pPD95.75. A 364bp *cho-1prom* (-3006, -2642; expressed strongly in AIA, AIY, AIN⁶¹) PCR fragment amplified from genomic DNA was cloned into MVC3 (*pSM::NLG-1::spGFP11*) and pPD95.75 to generate *cho-1prom::NLG-1::spGFP11* (pMM08) and *cho-1prom::mCherry* (pMM07), respectively. The constructs were injected at a total of 90 ng/μL, transgenic lines were picked based on the *mCherry* cytoplasmic expression, and the resulting extrachromosomal array strain was integrated into the genome using standard UV irradiation methods.

To generate the *rab-3* cytoplasmic reporter (*rab-3prom1::GFP*), *rab-3* promoter ("prom1"⁴) was cloned into pPD95.67 (plasmid containing *2xNLS-GFP*), where the *2xNLS* was removed. The resulting plasmid was injected as simple extrachromosomal array (50 ng/μL) into N2 animals, using *ttx-3prom::mCherry* as a co-injection marker (25 ng/μL). The resulting extrachromosomal array strain was integrated into the genome using standard UV irradiation methods. This was followed by 6 rounds of backcrossing to N2 to generate *otIs748*.

Automated worm tracking

Automated single worm tracking was performed using the Wormtracker 2.0 system at room temperature.²⁶ Young adult animals were recorded for 5 min and tracked on NGM plates with a small patch of food in the center (5 μL OP50 bacteria). Analysis of the tracking videos was performed as previously described.²⁶ For the tracking of the CUT rescue lines and controls, tracking was performed using the WormLab automated multi-worm tracking system (MBF Bio-science)²⁵ at room temperature. In each plate, 5 young adult animals were recorded for 5 min and tracked on NGM plates with a small patch of food in the center (5 μL OP50 bacteria). Videos were segmented to extract the worm contour and skeleton for phenotypic analysis. Raw WormLab data was exported to Prism (GraphPad) for further statistical analysis. Statistical significance between each group was calculated using One-way ANOVA followed by Tukey's multiple comparisons test.

Swimming analysis

The swimming assay was performed as previously described²⁹ using the WormLab automated multi-worm tracking system (MBF Bio-science)²⁵ at room temperature. In brief, 5 young adult animals were transferred into 50 μ l M9 buffer and recorded for 1 min. Multiple features of the swim behavior were then analyzed using the WormLab software. Swimming metrics are based on the metrics described in Restif et al.²⁹ WormLab data was exported to Prism (GraphPad) for further statistical analysis.

Aldicarb assays

Aldicarb assays were performed as previously described.⁵¹ Briefly, 25 young adult animals (24 h after L4 stage, blinded for genotype) were picked into freshly seeded NGM plates containing 1 mM aldicarb (ChemService). Worms were assayed for paralysis every 30 min by prodding with a platinum wire. A worm was considered paralyzed if it did not respond to prodding to the head and tail three times each at a given time point. Strains were grown and assayed at room temperature. Statistical significance between each group was calculated in Prism (GraphPad) using Two-way ANOVA followed by Tukey's multiple comparisons test.

Microscopy

Worms were anesthetized using 100 mM of sodium azide and mounted on 5% agarose on glass slides. All images were acquired using a Zeiss confocal microscope (LSM 880). Image reconstructions were performed using Zen software tools. Maximum intensity projections of representative images were shown. Fluorescence intensity was quantified using the ImageJ software.⁵³ Figures were prepared using Adobe Illustrator.

INTACT for purification of affinity-tagged neuronal nuclei

UPN::INTACT control worms (*otIs790*) as well as CUT sextuple mutant were grown on large plates (150mm) with enriched peptone media coated with NA22 bacteria to allow for the growth of large quantities of worms: 100,000 worms can grow from synchronized L1 stage to gravid adults on a single plate. ~600,000 animals were collected for each replicate at the L1 larval stage after egg preparation according to standard protocol. Animals were washed off the plate with M9, washed 3x with M9, lightly fixed with cold RNase-free DMF for 2 minutes before washing with 1xPBS 3x. We followed the modified INTACT protocol³³ to optimize pull-down of neuronal nuclei. All steps following were done in cold rooms (4 °C) to minimize RNA and protein tag degradation. The animals were homogenized mechanically using disposable tissue grinders (Fisher) in 1x hypotonic buffer (1x HB: 10 mM Tris pH 7.5, 10 mM NaCl, 10 mM KCl, 2 mM EDTA, 0.5 mM EGTA, 0.5 mM Spermidine, 0.2 mM Spermine, 0.2 mM DTT, 0.1% Triton X-100, 1x protease inhibitor). After each round of mechanical grinding (60 turns of the grinder), the grinder was washed with 1 mL 1x HB and the entire homogenate was centrifuged at 100xg for 3 min. The supernatant was collected for later nuclei extraction and the pellet was put under mechanical grinding and centrifugation for 4 additional rounds. The supernatant collected from each round were pooled, dounced in a glass dounce, and gently passed through an 18-gauge needle 20x to further break down small clumps of cells. The supernatant was then centrifuged at 100xg for 10 min to further remove debris and large clumps of cells. Nuclei was isolated from the supernatant using Optiprep (Sigma): supernatant after centrifugation was collected in a 50mL tube, added with nuclei purification buffer (1x NPB: 10 mM Tris pH 7.5, 40 mM NaCl, 90 mM KCl, 2mM EDTA, 0.5 mM EGTA, 0.5 mM Spermidine, 0.2 mM Spermine, 0.2 mM DTT, 0.1% Triton X-100, 1x protease inhibitor) to 20 mL, and layered on top of 5 mL of 100% Optiprep and 10 mL of 40% Optiprep. The layered solution was centrifuged at 5000xg for 10 min in a swinging bucket centrifuge at 4 °C. The nuclei fraction was collected at the 40/100% Optiprep interface. After removal of the top and bottom layers, leaving a small volume containing the nuclei, the process was repeated 2 additional times. After final collection of the crude nuclei fraction, the volume was added to 4 mL with 1xNPB and precleared with 10 μ L of Protein-G Dynabeads and 10 μ L of M270 Carboxylated beads for 30 min to 1 h (Invitrogen). The precleared nuclei extract was then removed, and 50 μ L was taken out as input samples (total nuclei). The rest was incubated with 30 μ L of Protein G Dynabeads and 3 μ L of anti-FLAG M2 antibody (Sigma) overnight to immunoprecipitate (IP) the neuronal nuclei. The following day, the IPed neuronal nuclei/beads were washed 6-8 times with 1xNPB for 10-15 min each time. The resulting IPed neuronal nuclei/beads were resuspended in 50 μ L 1xNPB and a small aliquot was used to check with DAPI staining to quality-check the procedure for the following: 1) sufficient quantities of nuclei was immunoprecipitated; 2) nuclei are intact and not broken; 3) the majority of bound nuclei are single, mCherry-labelled neuronal nuclei and minimal nuclei clumps and large tissue chunks were immunoprecipitated. Anything not satisfying these quality checks were not used for downstream processing. The resulting input and neuronal IP samples were used for isolation of total RNA using Nucleospin RNA XS kit according to manufacturer's protocol (Takara).

RNA-seq and data analysis

RNA-seq libraries were prepared using the Universal RNA-seq kit (Tecan) according to manufacturer's protocol. The libraries were sequenced on Illumina NextSeq 500 machines with 75bp single-end reads. After initial quality check, the reads were mapped to WS220 using STAR⁵⁴ and assigned to genes using featurecounts.⁵⁵ Differential gene expression analysis was conducted using DESeq2.¹⁸ 3834 genes were found to be differentially expressed in CUT sextuple mutants compared to wild-type animals (FDR < 0.05) (Data S2A). Gene Ontology and Phenotype Enrichment Analysis were performed using the Gene Set Enrichment Analysis tool from Wormbase (<https://wormbase.org>)⁵⁶ (Data S4A-S4D).

ChIP-seq datasets analysis

The CEH-48 ChIP-seq dataset (Experiment: ENCSR844VCY, bigBed file containing peak information: ENCFF784CKU) was obtained from the ENCODE portal (<https://www.encodeproject.org/>). The CEH-38 ChIP-seq dataset (Accession # modEncode_4800, gff3 interpreted data file containing peak information for combined replicates) was obtained from the modENCODE portal (<http://www.modencode.org/>). To identify the genes associated with these peak regions, peak coordinates were intersected with gene promoter regions (defined as from 5kb upstream of the transcription start site to 1kb downstream), and overlapping genes were identified (Data S1A–S1C). The consensus binding motif for CEH-48 and CEH-38 was obtained using MEME-ChIP,¹⁷ which returned similar motifs for both factors (consensus AATCGATA). Comparison of these motifs, and of the CEH-48 motif defined in Weirauch et al.,²⁰ to known motifs using the Tomtom Motif Comparison Tool in MEME Suite¹⁹ returned matches to known motifs for other ONECUT and CUX proteins (Data S6A–S6C).

QUANTIFICATION AND STATISTICAL ANALYSIS

All microscopy fluorescence quantifications were done in the ImageJ software.⁵³ For all images used for fluorescence intensity quantification, the acquisition parameters were maintained constant among all samples (same pixel size, laser intensity), with control and experimental conditions imaged in the same imaging session. For quantification of head neurons (Figures 2 and 3), nerve ring neurons (Figures S1 and S6) and ventral nerve cord neurons (Figure 6I), fluorescence intensity was measured in maximum intensity projections using a single rectangular region of interest. A common standard threshold was assigned to all the control and experimental conditions being compared. For quantification of individual neurons (Figure 6), fluorescence intensity was measured in the focal plane with the strongest neuronal nucleus signal within the z-stack (circular region of interest around the nucleus). For each worm, a single circular region of interest was also used to measure the background intensity in an adjacent area, and this value was then subtracted from the reporter fluorescence intensity value. For quantification of GFP::CLA-1 and GRASP puncta (Figure 4), manual counting was performed using the ImageJ software. For quantification of hypodermal cells (Figure S6), fluorescence intensity was measured as described above for individual neurons. For each worm five hypodermal cells were measured, and the fluorescence intensity averaged. The same hypodermal cells were measured in all animals compared.

For fluorescence quantification of CUT rescue lines (Figure 3), synchronized day 1 adult worms were grown on NGM plates seeded with OP50 and incubated at 20°C. The COPAS FP-250 system (Union Biometrica; “worm sorter”) was used to measure the fluorescence of 40–150 worms for each strain.

For all behavioral assay, randomization and blinding was done wherever possible. All statistical tests for fluorescence quantifications and behavior assays were conducted using Prism (Graphpad) as described in figure legends.